

DYNAMICS AND IMAGING OF SUBDUCTION

by

LELAND O'DRISCOLL

A DISSERTATION

Presented to the Department of Geological Sciences  
and the Graduate School of the University of Oregon  
in partial fulfillment of the requirements  
for the degree of  
Doctor of Philosophy

June 2012

DISSERTATION APPROVAL PAGE

Student: Leland O'Driscoll

Title: Dynamics and Imaging of Subduction

This dissertation has been accepted and approved in partial fulfillment of the requirements for the Doctor of Philosophy degree in the Department of Geological Sciences by:

Eugene Humphreys	Chairperson
Rebecca Dorsey	Member
Douglas Toomey	Member
Andrew Marcus	Outside Member

and

Kimberly Andrews Espy	Vice President for Research & Innovation/Dean of the Graduate School
-----------------------	--

Original approval signatures are on file with the University of Oregon Graduate School.

Degree awarded June 2012

© 2012 LELAND JAMES O'DRISCOLL

## DISSERTATION ABSTRACT

Leland O'Driscoll

Doctor of Philosophy

Department of Geological Sciences

June 2012

Title: Dynamics and Imaging of Subduction

Convergent plate boundaries evolve through the dynamic interaction between subducting oceanic lithosphere, overriding lithosphere, and adjacent flow of the convective mantle. These lithospheric plates contain remarkable heterogeneity in thickness, strength, and observable seismic character. I investigate the role of variable thickness of continental lithosphere with respect to mantle flow dynamics and develop a relationship of this subduction configuration with the construction of the Andes Mountains. By inclusion of this geodynamic model into the Andean Orogeny, numerous irreconcilable observations in the Eocene and Oligocene can be related with a comprehensive tectonic model.

Lithospheric heterogeneity can be imaged with the inversion of seismic travel time data. I develop an analysis of a potential source of non-unique modeling of seismic velocity structure and then develop a case study of a currently subducting oceanic lithosphere using an iterative ray tracing approach. First, I consider the impact of the assumption of isotropic wave propagation implicit in a common methodology of data inversion. First-order structure is shown to be well resolved, but higher-order structure can be significantly different in regions of observed high-amplitude or null SKS splitting observations.

The southern edge of the Juan de Fuca plate is imaged by traditional methods and an iterative ray tracing approach. The inclusion of ray tracing allows modeling of a more realistic velocity model by minimizing the error in source to receiver sensitivity. Compared to the standard imaging procedure, the resolved structure with this updated method contains smaller, more confined anomalies that represent the subducted oceanic lithosphere. Velocity perturbation amplitudes generally are decreased for slow structure and increase for fast structures. These changes in velocity structure provide an explanation for the decreased root mean square residual of the data that remain after inversion. I find that the high amplitude fast velocity of the Juan de Fuca is a robust feature and the currently subducting slab does not penetrate the mantle transition zone. I attribute the locus of very fast Juan de Fuca sub-continental lithosphere to be related to deformation of the plate prior to and during subduction.

This dissertation includes previously published co-authored material.

## CURRICULUM VITAE

NAME OF AUTHOR: Leland O'Driscoll

### GRADUATE AND UNDERGRADUATE SCHOOLS ATTENDED:

University of Oregon, Eugene, Oregon  
University of New Orleans, New Orleans, Louisiana  
Humboldt State University, Arcata, California  
College of the Redwoods, Eureka, California

### DEGREES AWARDED:

Doctor of Philosophy, Geological Sciences, 2012, University of Oregon  
Master of Science, Geology, 2006, University of New Orleans  
Bachelor of Arts, Geology, 2003, Humboldt State University  
Associate of Arts, 2001, College of the Redwoods

### AREAS OF SPECIAL INTEREST:

Subduction dynamics  
Teleseismic tomographic imaging  
Seismic anisotropy  
Structural geology, ductile strain behavior  
Granite geochemistry, emphasis on crustal differentiation  
Field geology, mapping

### PUBLICATIONS:

- O'Driscoll, L. J., M. A. Richards, E. D. Humphreys (2012), Nazca-South America interactions and the late Eocene-late Oligocene flat-slab episode in the central Andes, *Tectonics*, 31, TC2013, doi:10.1029/2011TC003036
- O'Driscoll, L. J., E. D. Humphreys, B. Schmandt (2011), Time corrections to teleseismic P delays derived from SKS splitting parameters and implications for western U.S. P-wave tomography, *Geophys. Res. Lett.*, 38, L19304, doi:10.1029/2011GL049031
- O'Driscoll, L. J., E. D. Humphreys, F. Saucier (2009), Subduction adjacent to deep continental roots: Enhanced negative pressure in the mantle wedge, mountain building and continental motion, *Earth Planet. Sci. Lett.*, 280, 61-70, doi:10.1016/j.epsl.2009.01.020

## ACKNOWLEDGMENTS

I first and foremost thank my parents Lee O’Driscoll and Melodee Sewell for encouraging me to pursue and supporting my pursuit of higher education. My growth as a scientist has been most significantly developed under the guidance of Eugene Humphreys. Interaction with Terry Pavlis, Doug Toomey, Rebecca Dorsey, Brandon Schmandt and Todd LaMaskin, Mark Hemphill-Haley and Brandon Schwab rounded out the breadth of my scientific perspective. I would not have developed the degree of interest in Earth Science to pursue a doctoral degree without a foundation provided by the Geology department at Humboldt State University. Time spent interacting with my father, farmers, ranchers and other land owners around California and Oregon led to appreciation of practical, tangible life skills. The pursuit of professionalism and personal challenge I developed while participating in competitive disc golf has been an invaluable activity that has provided an ideal parallel activity with respect to graduate research.

## TABLE OF CONTENTS

Chapter	Page
I. INTRODUCTION .....	1
II. SUBDUCTION ADJACENT TO DEEP CONTINENTAL ROOTS: ENHANCED NEGATIVE PRESSURE IN THE MANTLE WEDGE, MOUNTAIN BUILDING AND CONTINENTAL MOTION.....	3
1. Introduction.....	3
2. Modeling.....	5
2.1. Description of Model .....	6
2.2. Results.....	10
2.2.1. Root Thickness.....	11
2.2.2. Subduction Velocity .....	14
2.2.3. Mantle Viscosity .....	14
2.2.4. Asthenospheric Thickness and Viscosity .....	16
2.2.5. 3-D Models Testing Effects of Along-Strike Root Width.....	17
2.2.6. Root Distance from Subduction Zone .....	20
2.2.7. Very Low Viscosity Mantle Wedge.....	21
3. Discussion.....	25
3.1. General Discussion .....	25
3.2. Influence of Cratonic Roots on Flat-Slab Subduction .....	27
3.3. Modeling Limits .....	29
4. Conclusions.....	30

Chapter	Page
III. NAZCA-SOUTH AMERICA INTERACTIONS AND THE LATE	
EOCENE-LATE OLIGOCENE FLAT-SLAB EPISODE IN THE CENTRAL	
ANDES .....	32
1. Introduction and Background.....	32
1.1. Andean Orogeny.....	33
1.2. Plate Motion History.....	34
1.3. Mechanisms of Developing Flat-Slab Subduction .....	36
2. Central Andean Tectonics and the Influence of South American Cratons.....	37
2.1. South American Shield and Cratons.....	37
2.2. Central Andean (10°-30° S) Episodes of Flat-Slab Subduction.....	38
2.3. The Andean Orogenies in the Cenozoic .....	40
2.3.1. Onset of a Compressional Margin.....	42
2.3.2. Flat-Slab Period in the Central Andes, Peru and Bolivia .....	42
2.3.3. Re-steepening of the Slab .....	43
2.3.4. Development of the Modern Andean System.....	44
3. Geodynamic Forces .....	46
3.1. “Stagnation Point” Conceptual Model.....	46
3.2. Root Suction Model.....	49
3.2.1. Summary of the Cratonic Root-Enhanced Suction Mechanism	49
3.2.2. Application to the Central Andes of South America.....	52

Chapter	Page
3.3. Crustal Buoyancy and Oceanic Plateau Subduction.....	56
3.3.1. Buoyant Lithosphere Subduction.....	56
3.3.2. Manihiki Plateau Fragment Subduction, Eocene Central Andes .....	57
3.3.3. Slab Buoyancy Estimate for the Manihiki Plateau.....	58
3.4. Slab Buoyancy vs. Mantle Wedge Suction.....	60
4. Comparison Between the Sevier/Laramide and Andean Orogenies .....	62
5. Some Remarks on Model Limitations.....	65
6. Conclusions .....	66
 IV. TIME CORRECTIONS TO TELESEISMIC P DELAYS DERIVED FROM SKS SPLITTING PARAMETERS.....	68
1. Introduction.....	68
2. Teleseismic P-wave Correction Times Based on SKS Splitting Parameters....	70
3. Western U.S. Teleseismic P-wave Travel-Time Corrections .....	72
4. Discussion .....	75
5. Conclusion .....	78
 V. CONCLUSIONS.....	80
REFERENCES CITED .....	81

## LIST OF FIGURES

Figure	Page
2.1. Model used to test the effects of continental roots on upper mantle dynamics in the region between the root and the subduction zone.....	7
2.2. Enlargement of the high-resolution 2-D model, showing comparison of the pressure in the mantle wedge area for the cases with (bottom) and without (top) a continental root.....	9
2.3. Dynamic stresses, showing effects that result from variations in root depth and other parameters. ....	13
2.4. Comparison of tractions acting on the continental lithosphere, for the case with a root that extends to 250 km depth (red) and without a root (blue).....	15
2.5. Compressive force (per meter of strike-parallel length) near the subduction zone in the continental plate, as a function of mesosphere viscosity. ....	16
2.6. Effects on continental compression and mantle-wedge pressure caused by varying asthenosphere properties. ....	18
2.7. Three-dimensional mesh, with top 140 km removed, showing mantle-wedge suction in the mid asthenosphere. ....	19
2.8. Mantle-wedge pressure and continental compression for models with roots of various along-strike widths, using the 3-D mesh shown in Fig. 7 .....	21
2.9. Effects on continental compression and mantle-wedge pressure caused by varying root width and location. ....	22
2.10. Amount of continental compression as a function of root along-strike half-width and root distance to the mantle wedge tip .....	23
2.11. Effects on continental compression and mantle-wedge pressure caused by the inclusion of a very low viscosity mantle wedge tip. ....	24
3.1. Tectonic map of South America .....	35
3.2. Summary of tectonic model, modified from <i>James and Sacks</i> [1999]. ....	41

Figure	Page
3.3. Timing of along-strike strain distribution across the central Andes, modified from <i>Arriagada et al.</i> [2008] .....	49
3.4. Summary of spatial scaling for modeled mantle wedge tip to craton edge distances .....	51
3.5. Finite element model representing South American cratonic configuration and comparison with our conceptual tectonic model .....	54
3.6. Reconstruction of the pathways of the Manihiki Plateau (white) and a conjugate fragment (black) .....	58
4.1. SKS field for the western U.S. Data compiled from <i>Liu</i> [2009] .....	69
4.2. Ratio of P delay caused by azimuthal anisotropy to the SKS split time, as a function of P-wave incidence angle and back azimuth.....	73
4.3. Interpolated map of P-wave arrival-time corrections estimated using the methods described in the text.....	74
4.4. Comparison of velocity models at 195 km depth .....	76

## CHAPTER I

### INTRODUCTION

In this dissertation, I investigate the role that lithospheric heterogeneity plays in the evolution of orogenic belts. Continental lithosphere is composed of thick and old interior portion, termed cratons, with fringing thin and younger lithosphere. The range in thickness is as great as 250 km in some of Earth's oldest continental masses. This heterogeneity can give rise to unique tectonic activity in relation to variation in strength and interaction with viscous mantle flow.

Another examination the nature of lithospheric heterogeneity is through imaging techniques that use earthquake energy. I evaluate the sensitivity of an assumption made during the process of seismic imaging that is related to anisotropic wave propagation.

Chapter II develops a generic model for the process of subduction beneath cratons. Various controlling parameters such as root geometry, mantle viscosity structure, and boundary conditions are examined. The modeling is conducted via three dimensional finite element simulations. This chapter is coauthored with my dissertation advisor Gene Humphreys and was published in *Earth and Planetary Science Letters*, 2009. Chapter III focuses on an application of the generic model to the tectonic evolution of the central Andes mountain range. With this effort, I develop an examination of the dynamic mechanisms that are attributed to subduction beneath craton-bearing continents. By placing the role of cratonic root-enhanced mantle wedge suction, I produced a verification of the generic model by establishing consistency with multi-disciplinary geologic records. In other words, the working hypothesis of my generic model was tested. I found that a unique period of shallow angle subduction and variation in

shortening and volcanic activity during the 40-25 Ma period in the Peruvian and Bolivian Andes was intimately related to the my subduction model. This work is coauthored by my colleague at UC Berkeley, Mark Richards, and my advisor Gene Humphreys, and was published in *Tectonics*, 2012.

Chapter IV investigates a major assumption of seismic imaging that is based on inversion of travel time anomalies. When inverting travel time delays to solve for velocity perturbation structure, it is common to assume that earthquake waves pass through the Earth according to an isotropic material property. In this case, the local velocity is constant for all directions of propagation of elastic energy. This chapter begins with a scaling of the most common analysis of mantle anisotropy, shear-wave splitting analysis. For the entire western United States, I develop a scaling relationship between the shear-wave splitting field and travel time delays that are used in the tomographic inversion scheme that allows imaging of velocity structure. I demonstrate that to a first-order the velocity structure that results from the assumption of isotropic material property is not significantly affected. However, finer-scale structure can be significantly affected, especially in the case of high lateral gradients in observed anisotropy. I also develop a relationship between the orientation of anisotropy in three-dimensional mantle structure and teleseismic wave propagation, and argue that regions of vertical flow in the mantle are much more sensitive to the assumption of isotropic velocity. This analysis provides a framework for future research that I am currently undertaking. This chapter was coauthored with my advisor Gene Humphreys and Brandon Schmandt, and was published in *Geophysical Research Letters*, 2011.

## CHAPTER II

# SUBDUCTION ADJACENT TO DEEP CONTINENTAL ROOTS: ENHANCED NEGATIVE PRESSURE IN THE MANTLE WEDGE, MOUNTAIN BUILDING AND CONTINENTAL MOTION

Reproduced with permission from Humphreys, E.; Saucier, F. *Earth and Planetary Science Letters*, **2009**, 280, 61-70. Copyright 2009, Elsevier.

### 1. INTRODUCTION

The occurrence of strongly compressional orogens that maintain high (>3 km) orogenic plateaus is not especially surprising in areas of continental convergence (e.g., Himalayan and Appalachian orogenic belts). More enigmatic are similar orogens created during subduction of oceanic plate beneath continents (e.g., Cordilleran orogenies of the western Americas). These orogenies are not explained easily by typical subduction, and special subduction conditions usually are inferred such as slab flattening (van Hunen et al., 2004), subduction of thickened oceanic crust (Gutscher et al., 2000; Saleeby, 2003), unusually rapid continental motion over the subduction zone (English and Johnston, 2004; Victor et al., 2004) or slab anchoring in the lower mantle (Zhong and Gurnis, 1995).

Our study is motivated by observations of apparent rapid trenchward motion of North America during the Laramide orogeny (Engebretson et al., 1985; Jarrard, 1986) and of South America during the Andean orogeny (Silver et al., 1998; Somoza,

1998). During the Laramide, North America accelerated to absolute velocities  $> 4$  cm/yr (Engebretson et al., 1985; Gordon and Jurdy, 1986) while Rocky Mountain compressive tectonics occurred  $> 1000$  km from the subduction zone. Similarly, South America absolute plate velocity increased during the highly compressive Andean orogeny of the last 50 m.y. (Gordon and Jurdy, 1986; Pardo-Casas and Molnar, 1987; Silver et al., 1998; Sobolev and Babeyko, 2003; Almendinger et al., 1997). From a plate-wide perspective, strong compression on the western margin of the continent would normally be expected to resist and slow westward plate motion (Iaffaldano and Bunge, 2008). Considering that ridge activity on the eastern margin of the plate apparently was not anomalous (Lawyer and Müller, 1994; Müller et al., 2008, Cande et al., 1995), an additional force is needed to move the continental plate more rapidly while simultaneously overcoming the increased resistance of relatively great magnitude on its leading edge. Common features of the Laramide and Andean orogenies include the presence of large cratonic roots above a downgoing slab and the occurrence of continental thrusting across the width of the continent between the root and the subduction zone. These features lead us to focus on the influence of the cratonic root in the subduction process.

Subduction entrains mantle flow with the descending slab, creating suction (negative pressure) in the mantle wedge (Stevenson and Turner, 1977; Tovish et al., 1978). The suction draws asthenosphere into the subduction corner from below the overriding plate, which establishes a corner flow within the wedge. The magnitude of the negative pressure depends on subduction velocity, mantle viscosity, and slab

geometry. A low asthenosphere viscosity reduces impedance to asthenospheric flow into the wedge, thereby reducing the magnitude of the suction (Manea and Gurnis, 2007). Subduction beneath continents can be complicated by the presence of cratonic roots, which interfere with the flow of asthenosphere into the mantle wedge. Seismic images of cratons indicate that these roots extend to depths of 150-250 km (Grand, 1994; Gung et al., 2003). These root depths project near to or beyond the base of the asthenosphere (as it commonly is perceived).

We generate subduction models that examine the effects of the restricting supply of asthenosphere into the mantle wedge by the presence of deep cratonic lithospheric roots.

## 2. MODELING

To isolate and test the dynamic effects of a continental root on lithospheric stress and the forces applied to the continent, we perform a series of simple 2-D and 3-D numerical models to compare the stress state between a standard subduction model and those that include a lithospheric root but are otherwise identical. We find that a root can significantly enhance mantle wedge suction and broaden the low-pressure area to include the region between the root and subduction zone, provided that the root is closer than 300-500 km from the mantle wedge corner. This suction adds a strong component of compression to the continental lithosphere that lies between the root and the subduction zone, and it pulls the continent toward the subduction zone with a force that can be tectonically important.

Comparison among different subduction situations is made by monitoring stresses in the mantle wedge and within the continent. Because our modeling is of the instantaneous stress state, it does not address migrating plate boundaries or long-term evolution of the subduction system.

## 2.1. Description of model

We calculate instantaneous flow in rectangular coordinates by solving the momentum and continuity equations in three dimensions with the finite element method. This is accomplished with the Lagrangian finite element package ABAQUS, using linear hexahedral elements. ABAQUS uses viscoelastic elements, which are made effectively incompressible viscous by setting Poisson's ratio to 0.49 and time stepping until stress equilibrium is attained (which occurs rapidly). The inclusion of small amounts of compressibility results in a straightforward handling of pressure. In benchmark tests, calculated pressures and deviatoric stresses are indistinguishable from those known of analytic solutions.

Model parameterization (geometry and material properties) is represented in Fig. 2.1. The model is 2000 km deep by 2000 km wide, and 3-D models have an along-strike width of 2000 km. The continental and oceanic lithospheres have thicknesses of 100 km, and for models that contain a cratonic root, the root extends from the base of the lithosphere to depths of 150-350 km (with 250 km being our reference). Asthenosphere lies between depths of 100-200 km in most models (except where this volume is occupied by a cratonic root). Elements range in dimension from 5

km in the mantle wedge to 100 km near the margins of the model. The stability of calculations is tested by doubling the model resolution (with element dimensions ranging from 2 km to 50 km, as shown in Fig. 2.2). Resulting changes in stress values are an insignificant few percent, confirming adequate resolution with use of our standard mesh. The standard mesh is used in all figures shown below, except Fig. 2. 2.

The subducting oceanic slab extends to a depth of 800 km. Slab shape is chosen so that in the rootless case the negative buoyancy of the subducted slab

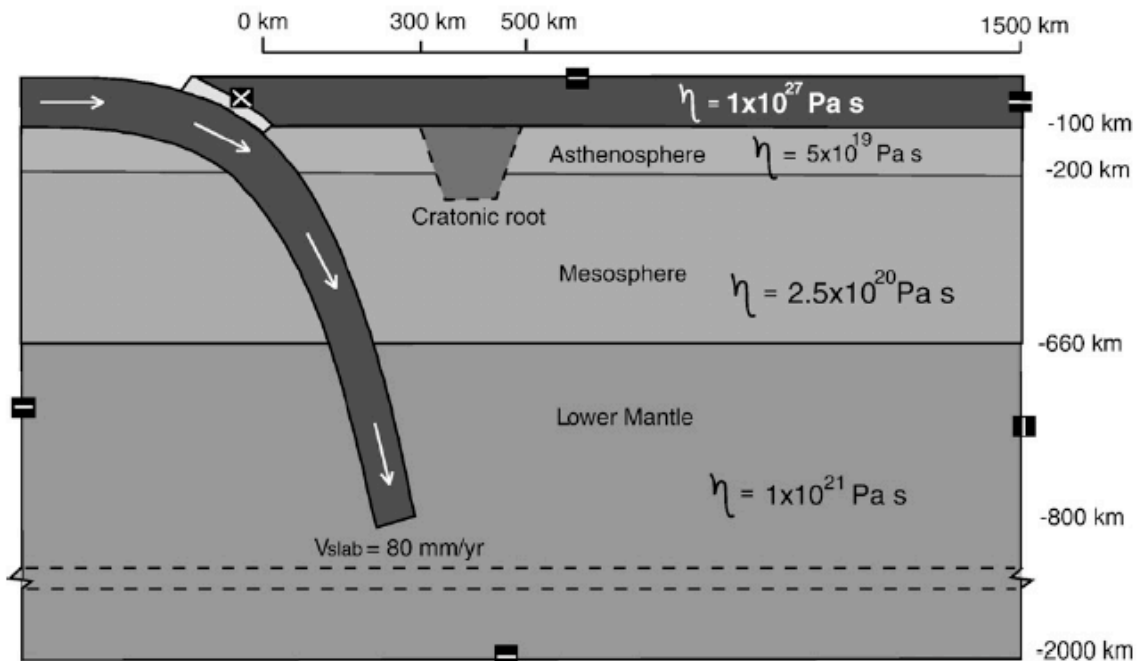


**Figure 2.1.** Model used to test the effects of continental roots on upper mantle dynamics in the region between the root and the subduction zone. Ocean plate extends to a depth of 800 km. Away from the slab and root, the layered structure of the reference model is: plates of viscosity  $10^{27}$  Pa·s extend to 100 km, asthenosphere of viscosity  $5 \times 10^{19}$  Pa·s extends to 200 km, upper mantle (mesosphere) of viscosity  $2.5 \times 10^{20}$  Pa·s extends to 660 km, and lower mantle of viscosity  $10^{21}$  Pa·s extends to the base of the model at 2000 km. Boundary conditions are indicated with the boxed symbols, which show direction of free slip or boundary that is held fixed. A narrow subduction channel accommodates subduction adjacent to the continent. Horizontal distance is measured from the mantle wedge tip. For modeled variations to this model, see Fig. 3 and the text.

(Ranalli et al., 2000) is approximately balanced by viscous tractions acting on the slab, resulting in a slab shape that is observed commonly (e.g., Jarrard, 1986; Lallemand et al., 2005). This produces a reference no-root model whose slab geometry is in steady-state subduction.

The distribution of material viscosity shown in Fig. 2.1 represents our standard model, from which we vary individual parameters. All elements are incompressible and Newtonian viscous. The continental plate has a high viscosity of  $10^{27}$  Pa·s so as not to deform significantly during modeling. In most models, the asthenosphere, upper mantle and lower mantle have viscosities of  $5 \times 10^{19}$ ,  $2.5 \times 10^{20}$  and  $10^{21}$  Pa·s, respectively. The effects of varying this viscosity structure are discussed below. Boundary conditions are indicated in Fig. 2.1. Flow is driven by the prescribed motion of the oceanic plate and slab. All points within the oceanic plate and slab move with uniform speed parallel to the slab margins, thereby maintaining slab shape. We hold fixed the left side of the continental plate at the subduction interface and include a zone of elements between the two plates in the subduction channel. The kinematically prescribed conditions on either side of the subduction channel fully decouple the motion of the subducting plate from the continent across the subduction zone. The prescribed motion on either side of this channel imposes simple shear deformation of the channel. Subduction channel elements are assigned a high viscosity ( $10^{27}$  Pa·s) to assure no flow into the mantle wedge. For our modeling, in which the plate motion past the leading edge of the continent is kinematically

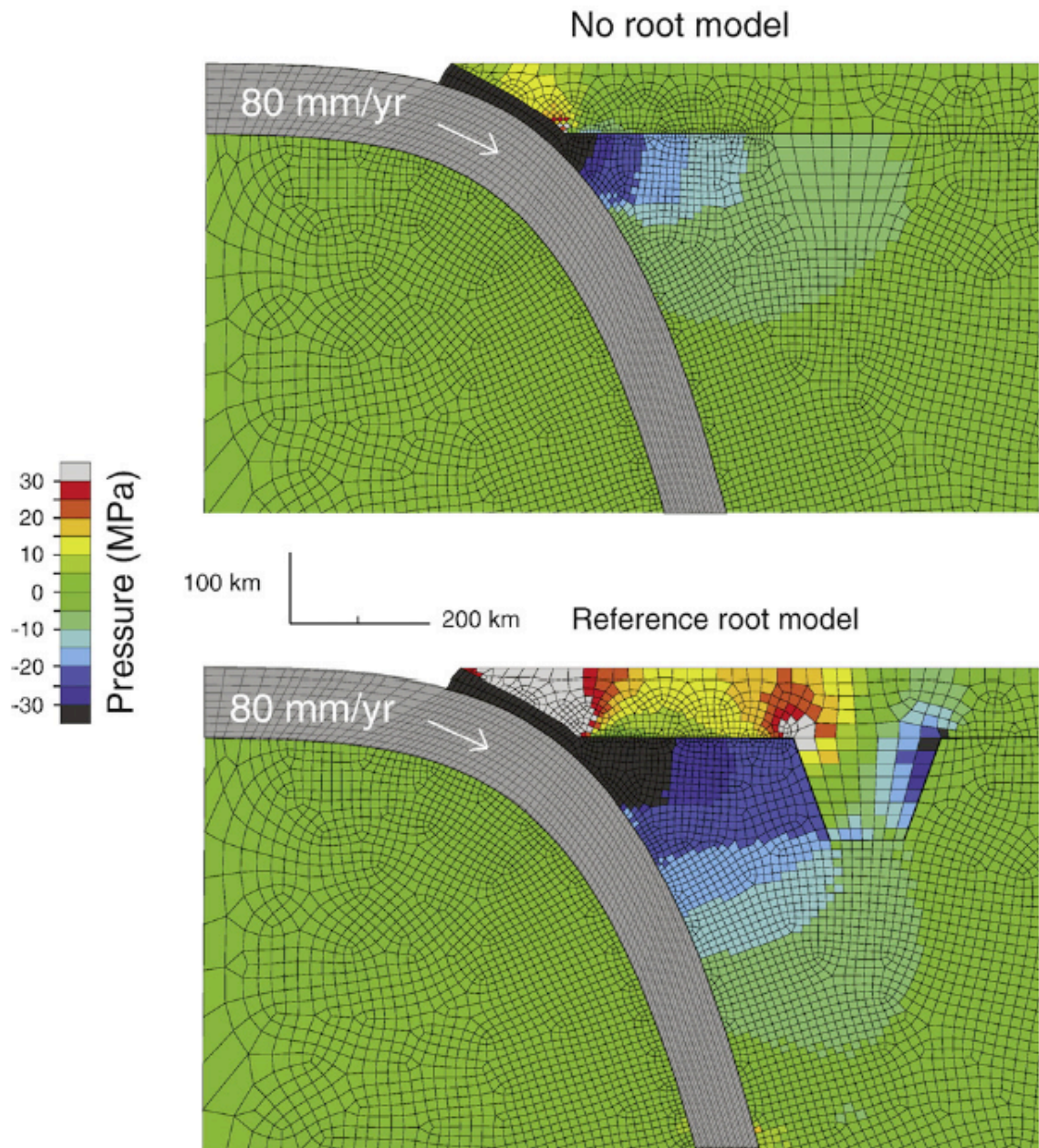


**Figure 2.2.** Enlargement of the high-resolution 2-D model, showing comparison of the pressure in the mantle wedge area for the cases with (bottom) and without (top) a continental root. Model parameters are described in Fig. 2.1. Inclusion of the root both increases the magnitude of the suction (negative pressure) and broadens the affected zone away from the subduction zone and to the margin of the root. Pressure in the continent between the root and the subduction zone is generally compressive and includes effects of flexure (which are not relevant to this study).

imposed, this treatment of the subduction channel is straightforward. Similar conditions can be met in Eulerian modeling of subduction, although more sophistication is needed (e.g., Billen and Gurnis, 2001).

Particle motion is free parallel to the boundaries, except on the left model boundary, the oceanic plate, and the right side of the continental plate. On the left boundary, only motion normal to the boundary is allowed. We use this condition so that the flow in the volume beneath the slab is not forced to flow in a small cell. Because slab motion is prescribed and we are interested in processes above the slab, the left-side boundary conditions do not influence our results. The horizontally free right side of the continent simulates an oceanic ridge there. For the sub-lithospheric mantle on the right side, a variety of boundary conditions have been tried ranging from completely free horizontal flow to no horizontal flow. We chose a no horizontal flow boundary condition there, although we find that the effect on flow and stress in the mantle wedge and on lithospheric stress are negligible.

## 2.2. Results

A set of 2-D models have been run to test the effects of a root, in which we vary root depth and its distance to the wedge corner, asthenosphere thickness and viscosity, and upper mantle viscosity. These tests are followed by a set of 3-D models in which along-strike root width also is varied, to examine the effects of 3-D flow and to understand how well the 2-D models capture the physics of 3-D subduction. Figure 2.2 illustrates with 2-D modeling the basic process involved with

the cratonic root. Notice the enhanced suction in the mantle wedge created by the cratonic root. By applying normal tractions on the root, this mantle-wedge suction couples more effectively to the continental plate than the case without a root, where only shear tractions applied by the flowing asthenosphere create coupling to the continent. To represent our suite of models, we show plots of trench-normal compression of the continental lithosphere and pressure in the mantle wedge. The net continental compression is calculated by integrating trench-normal normal stress across the 100-km thickness of the lithosphere (at a location 50 km to the left of the root). This force is both the additional force acting to drive the continent toward the subduction zone and it contributes to the contractional orogenies we wish to address. The negative pressure in the wedge is monitored to facilitate comparison between the suction in the mantle wedge and the continental compression. We choose a representative point within the mantle wedge that lies 50 km below the lithosphere and 80 km to the right of the slab at the same depth.

### 2.2.1. Root thickness

The amount of root penetration into and through the asthenosphere is varied in these models, but they are otherwise as shown in Fig. 2.1. Figure 2.2 shows mantle pressure field for a 2-D case without and with a root (for a root depth of 250 km). The presence of a root enhances the suction in the mantle wedge and expands the area of high suction to include all of the asthenosphere between the root and the wedge corner. Suction in the asthenosphere between the slab and the root increases in

magnitude by a factor of about two compared to the rootless model. Figure 2.3a shows how the magnitude of suction in the mantle wedge increases steadily as root thickness increases, and Fig. 2.3b shows how continental compression increases as the root depth increases. In Fig. 2.3b we have isolated the contributions to the net continental compression caused by shear force acting over the base of the root (labeled ‘Basal shear on root’) and horizontally directed pull on the left edge of the root (‘Root suck’) by integrating, respectively, the horizontal shear stresses acting over the width of the root and the horizontal stress acting on the left edge of the root (i.e., below the 100 km thickness of the lithosphere to the base of the root). The root suck force is seen to be the dominant cause of continental compression.

Figure 2.4a shows how vertical tractions on the continent overlying the mantle wedge are affected by the suction created by the root (obtained from the modeled vertical tractions at the base of the continent). As with the stresses acting on the root, stresses are evaluated in the mantle adjacent to the root. The enhanced suction pulls the continental lithosphere down, as indicated by the vertical tractions on the base of the lithosphere that become more negative by 15 MPa.

Inclusion of a root causes a strong compression in the continent between the subduction zone and the root (Fig. 2.4b). This compression increases strongly as the base of the root approaches the base of the asthenosphere and continues to increase as the root extends beyond the base of the asthenosphere (Fig. 2.3b). Compression of the continent increases from 1.4 TN/m (units of  $10^{12}$  Newtons per meter) in the across-strike direction with no root, to 5.1 TN/m with the root extending to 250 km

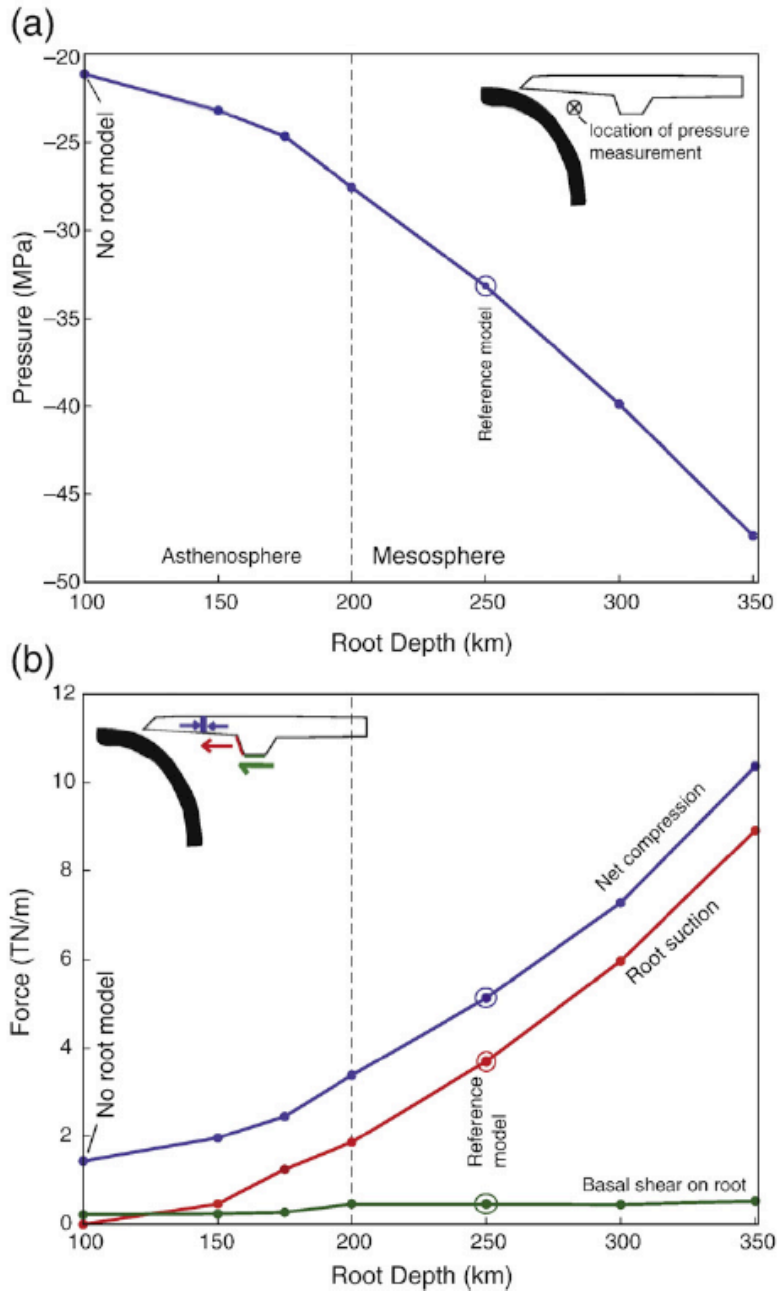


**Figure 2.3.** Dynamic stresses, showing effects that result from variations in root depth and other parameters. (a) Mantle-wedge pressure (suction) as a function of root depth, for a sample point in the mantle wedge at 150 km depth (center of the asthenosphere) and 80 km to the right of the slab. (b) Compressive force (per meter of strike-parallel length) in the continental plate and near the subduction zone, as a function of root depth. The case of no root is on the left side of the plot. The net compression is shown with the upper curve. The contributions to this compression owing to horizontal tractions on the root (root suck) and owing to basal shear on the root are shown.

(i.e., to 50 km beneath the base of the asthenosphere, Fig 2.3b). In all cases, the primary origin of continental compression is the pull on the root caused by the increased suction (Fig. 2.3b, labeled 'Root suck', red line). The remainder of continental compression is caused by horizontal basal tractions, both on the base of the root (see Fig. 2.3b, green line) and along the base of the continent away from the root. Enhanced continental compression is confined to the region to the left of the root (Fig. 2.3d).

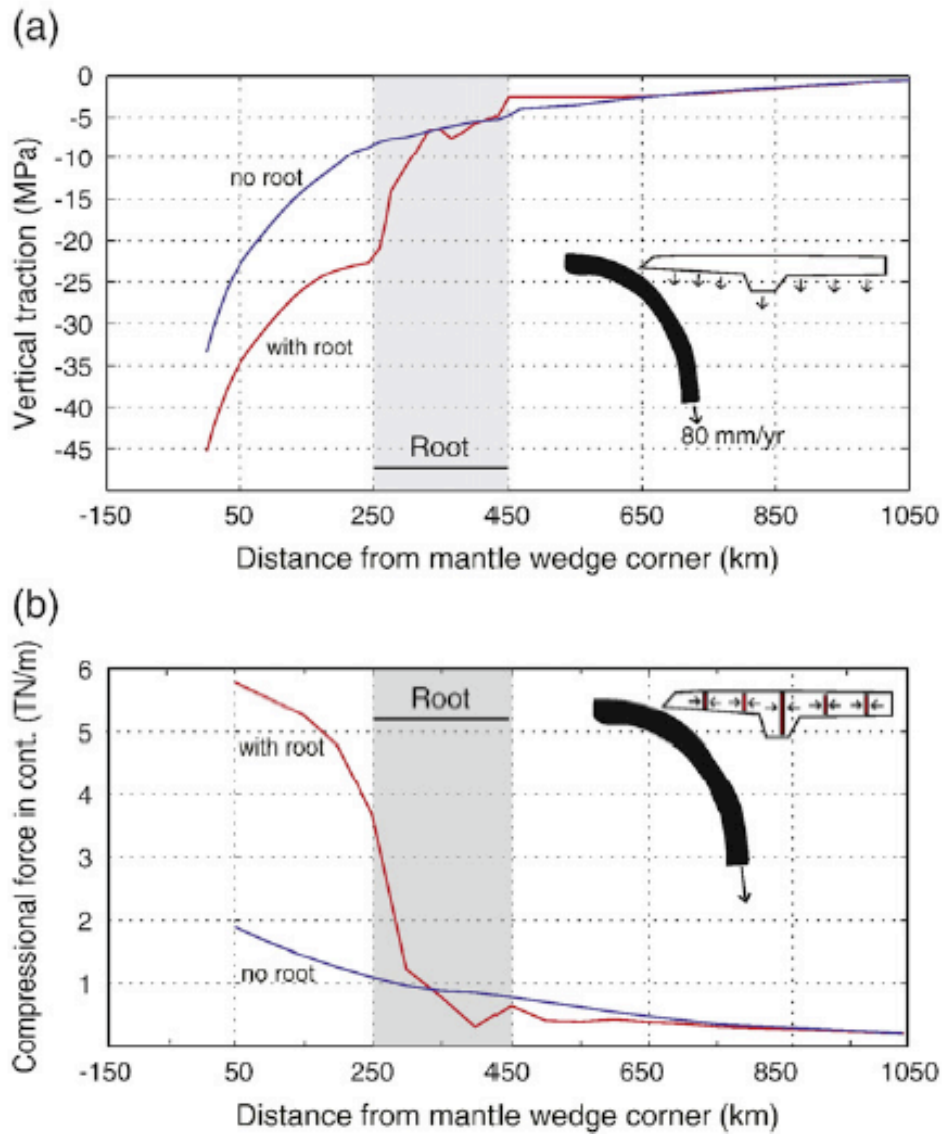
### 2.2.2. Subduction velocity

We have assumed a subduction velocity of 80 mm/yr, similar to young Nazca-South America plate convergence (Gordon and Jurdy, 1986, Iaffaldano and Bunge, 2008). (Antarctic plate subduction beneath southern Chile, at ~20 mm/yr, is slow.) All the dynamic effects modeled in our study are linearly proportional to subduction velocity. For instance, a subduction velocity of 120 mm.yr, which may be more representative of the Laramide orogeny (Engelbreton et al., 1985; Stock and Molnar, 1988), would have stresses and forces that are 50% greater than those shown in this paper.

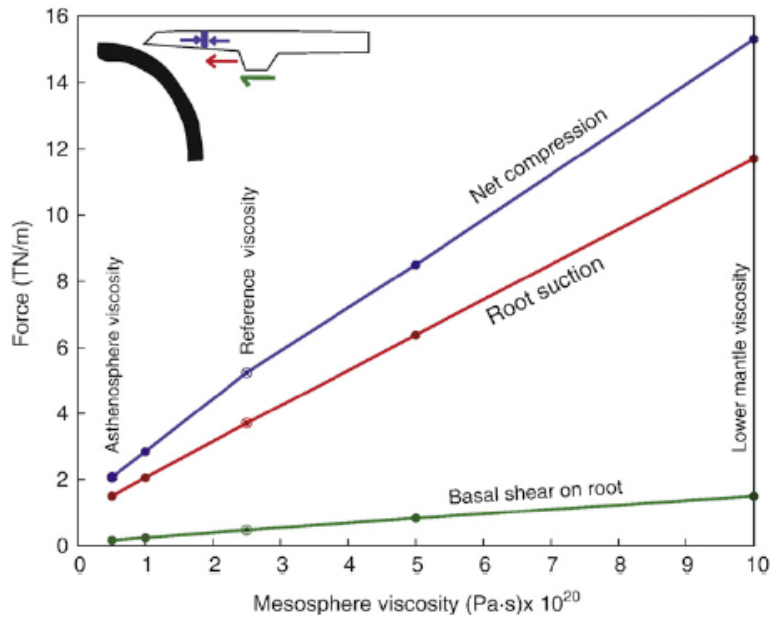
### 2.2.3. Mantle viscosity

Figure 2.5 shows the effects of varying the viscosity of the mesosphere (mantle between the asthenosphere and the lower mantle) for models that are

otherwise as shown in Fig. 2.1. The effects of the root on continental compression are nearly linear on mesosphere viscosity. A mesosphere viscosity of  $2.5 \times 10^{20}$  Pa·s creates a continental compression of 5 TN/m.



**Figure 2.4.** Comparison of tractions acting on the continental lithosphere, for the case with a root that extends to 250 km depth (red) and without a root (blue). (a) Vertical traction acting on the base of the continent as a function of distance from the trench. (b) Compressive force (per meter of strike-parallel length) in the continental plate, as a function of distance from the trench.



**Figure 2.5.** Compressive force (per meter of strike-parallel length) near the subduction zone in the continental plate, as a function of mesosphere viscosity. The left side is for an iso-viscous upper mantle, and the right side is for all sub-asthenospheric mantle equaling our lower mantle viscosity.

#### 2.2.4. Asthenosphere thickness and viscosity

As asthenosphere thickness increases, both mantle wedge suction and continental compression diminish (Fig. 2.6). This is especially pronounced when the base of the asthenosphere extends below the craton root (Fig 2.6c). When the asthenosphere is thin compared to root depth and becomes confined to the cavity created between the root and subducting slab; then, mesosphere evacuated by slab subduction must create the large suction required to pull in mesosphere from around the root and replace the evacuated mantle.

When roots penetrate the asthenosphere, variations in asthenosphere viscosity are not very significant. Reductions in asthenospheric viscosity by an order of magnitude below the reference value causes reduction in mantle-wedge suction and continental compression of ~15% (Fig. 2.6a-b). Increasing asthenospheric viscosity to values equal to the mesosphere viscosity results in a ~20% increase continental compression and a ~60% increase in mantle wedge suction for our reference case of a root extending to 250 km depth.

#### 2.2.5. 3-D models testing effects of along-strike root width

A root of finite along-strike width allows asthenosphere to flow around the root and enter the low-pressure area of the wedge from the sides. This reduces wedge suction and lithospheric stress. In this section we test the sensitivity and behavior of mantle-wedge pressure and continental compression on root width. Model results indicate that 3-D subduction physics is similar to that in 2-D, but that the magnitude of the root effects is less intense.

Figure 2.7 provides a 3-D perspective on the mantle-wedge pressure and trench-normal horizontal lithostatic compression for a model in which root half-width is 900 km. The root is placed against a reflecting boundary on the front side, simulating the case of a symmetrical root that is twice that of our model. Mantle-wedge pressure and continental compression on the front plane are nearly those obtained in the 2-D root model, and that on the back plane they are nearly those obtained in the 2-D no-root model. Model width is chosen so that the side boundary

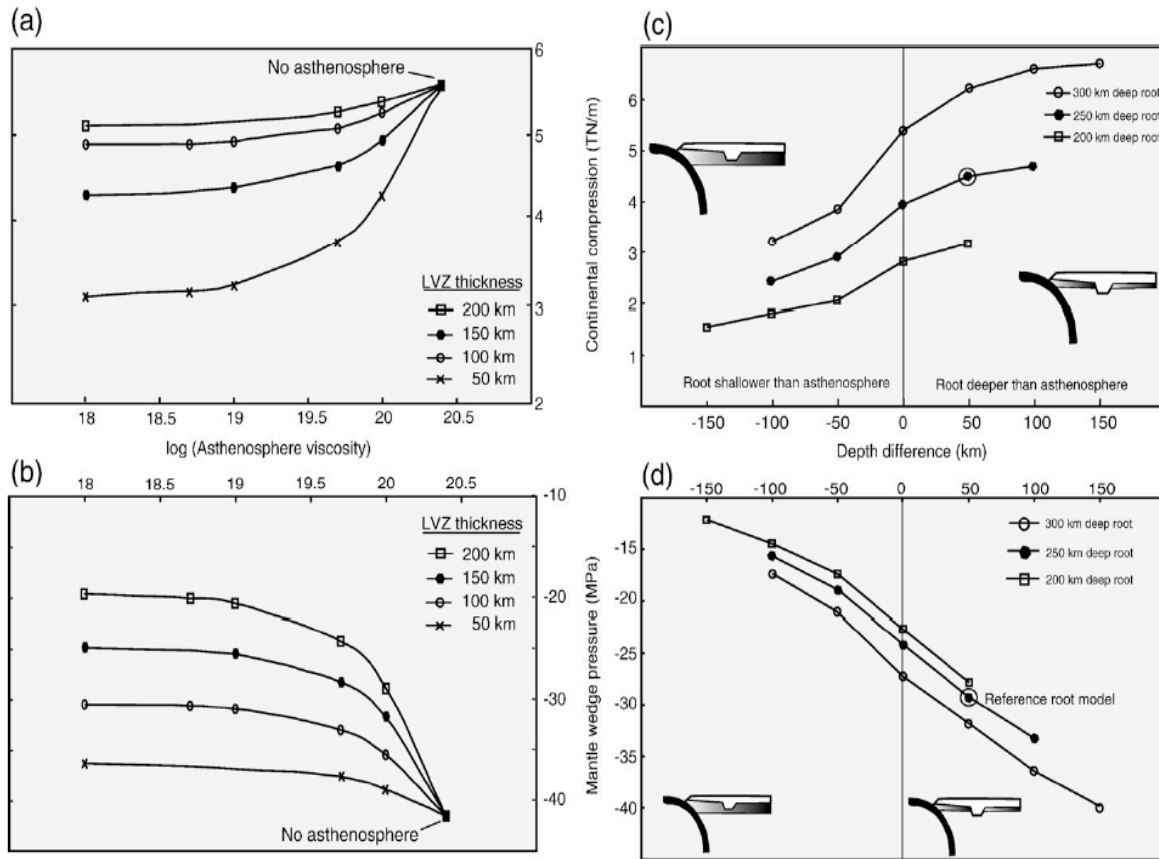


**Figure 2.6.** Effects on continental compression and mantle-wedge pressure caused by varying asthenosphere properties. (a) Continental compression as a function of asthenosphere viscosity for several thicknesses of asthenosphere (below the 100-km thick lithosphere). (b) Mantle wedge pressure as a function of asthenosphere viscosity for several thicknesses of asthenosphere. (c) Continental compression as a function of root depth minus depth to the base of the asthenosphere (i.e., root penetration depth) for three root depths. (d) Mantle wedge pressure as a function of root penetration depth, for three root depths.

away from the root has negligible effect on the results, as determined by running a set of models with various along-strike model widths. For all modeled root widths (200, 500 and 900 km), the dynamics at the back plane (away from the root) are similar to the 2-D rootless case.

Fig. 2.8a shows the variation in mantle-wedge pressure along a line that corresponds with the point chosen in the 2-D modeling. Mantle-wedge suction is transitional between the 2-D root case and the 2-D no-root case, and for root widths

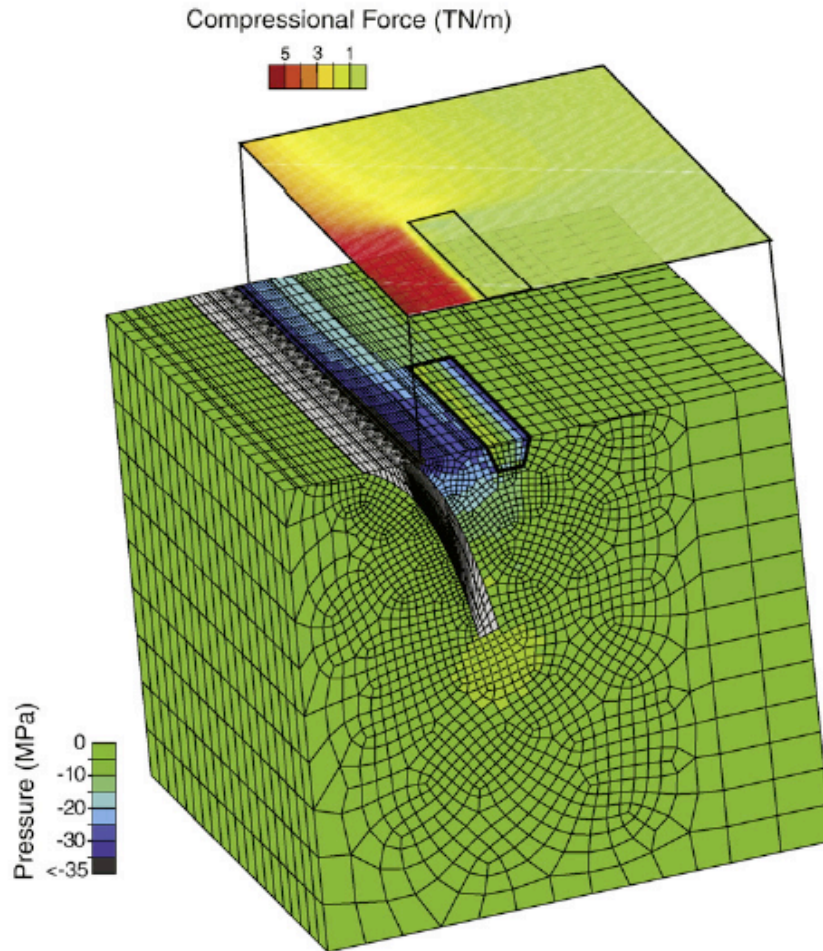


**Figure 2.7.** Three-dimensional mesh, with top 140 km removed, showing mantle-wedge suction in the mid asthenosphere. The boundary condition on the front face is reflecting; other boundary conditions are as described in Fig. 2.1 for the 2-D model. The surface above the mesh shows trench-normal continental compression integrated through the lithosphere.

greater than 500 km the suction effects at the root center are greater than 80% of those in the 2-D root case. Fig. 2.8b shows the horizontal continental compression for the same three root widths. When along-strike root half-width is greater than  $\sim 500$  km,

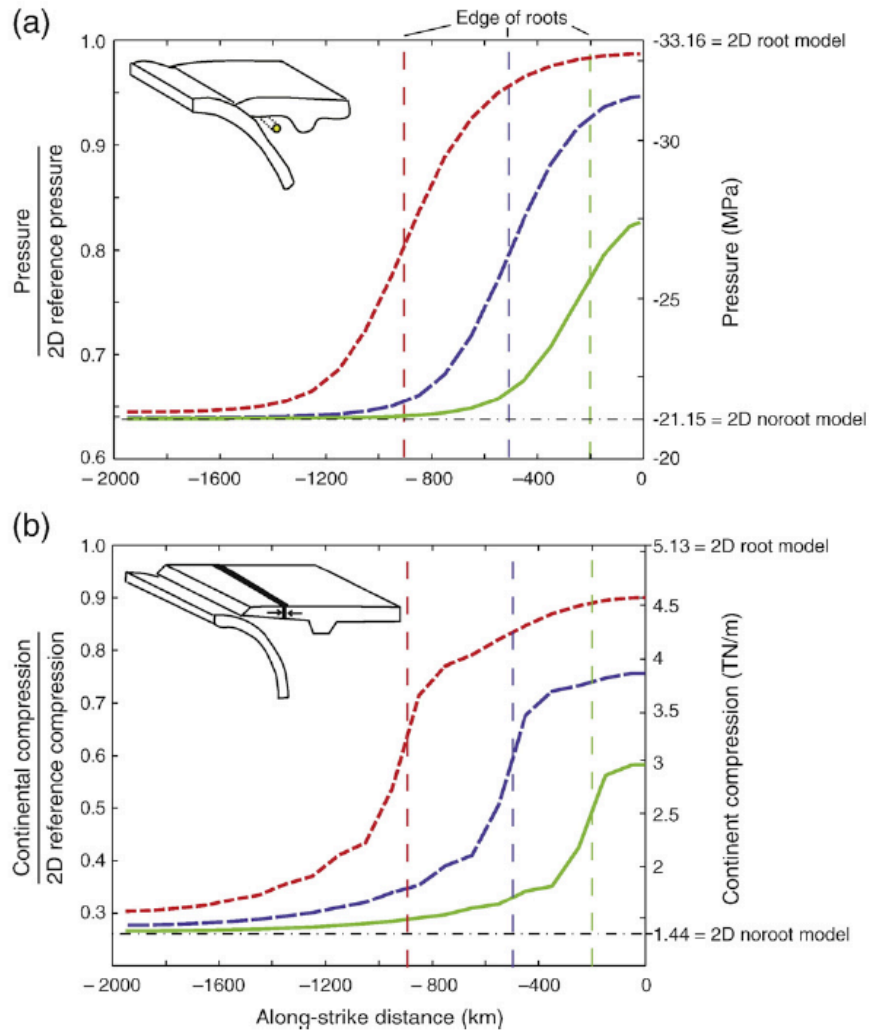
conditions near the root center approach the case of the 2-D root. Stress magnitudes approach those of the 2-D case with increasing along-strike root width, and for a given root width, the point where the effects of the root are half their maximum value is near the edge of the root (Fig. 2.8). A root of 200 km half-width reduces mantle-wedge pressure and increases lithospheric compression at the root center by an amount that is about half that experienced by the infinite-width (2-D) root. By 900 km half width, the middle half of the root experiences stresses nearly that of the infinite-width root (Fig. 2.8).

#### 2.2.6. Root distance from subduction zone

For the set of root widths modeled above, we varied the root location relative to the subduction zone. The results are shown in Fig. 2.9. When the separation between the root and the mantle wedge tip exceeds  $\sim 400$  km, the dynamic effects of the root become greatly reduced; when the root is 900 km from the wedge tip, its effects are minor. Mantle-wedge suction and continental compression each diminish as the root is narrowed and as it is moved away from the subduction zone, with the latter effect being the most important (Fig. 2.10). For instance, continental compression in our 2-D reference model (Fig. 2.1, which has the root located 300 km inboard of the mantle-wedge corner) is elevated by 3.7 TN/m compared to the rootless model. This amount of additional continental compression is reduced to 2 TN/m (at the root's along-strike center) either by narrowing the root to  $\sim 600$  km width or by locating the root  $\sim 500$  km from the mantle-wedge corner (Fig. 2.10).

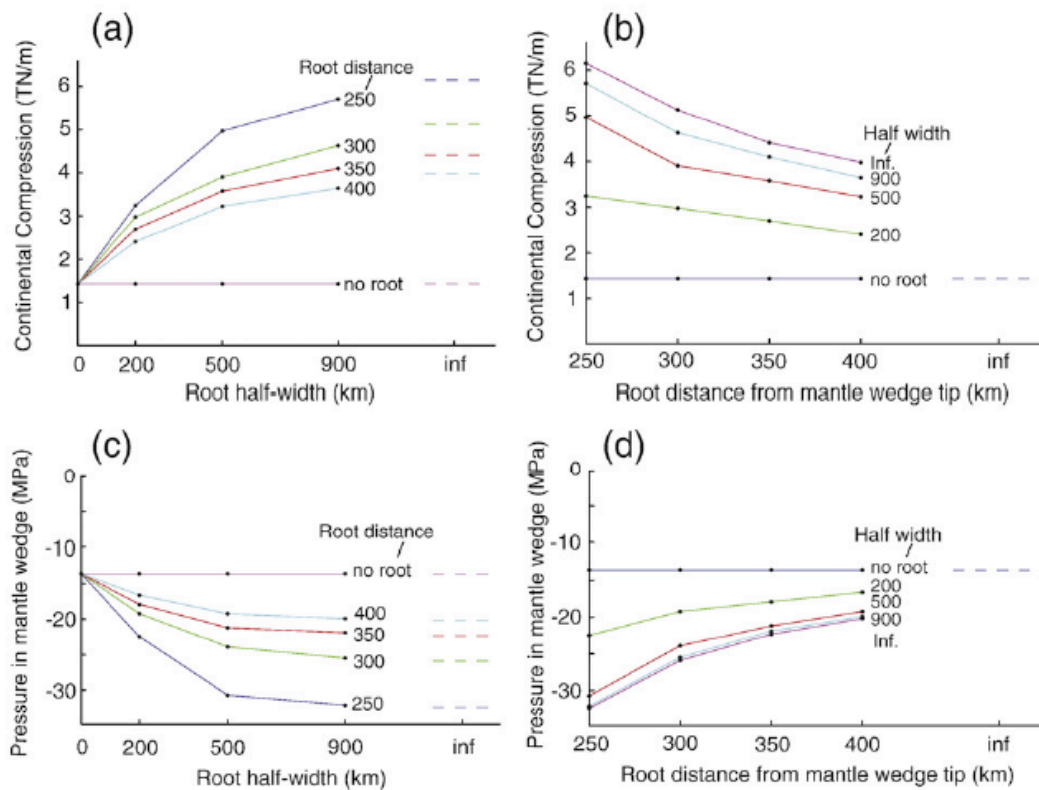
### 2.2.7. Very-low viscosity mantle wedge

Billen and Gurnis (2001) found that very low viscosities are necessary to account for the geoid and dynamic topography over the mantle wedge. We have modeled their preferred mantle-wedge geometry with a viscosity of  $10^{18}$  Pa·s.



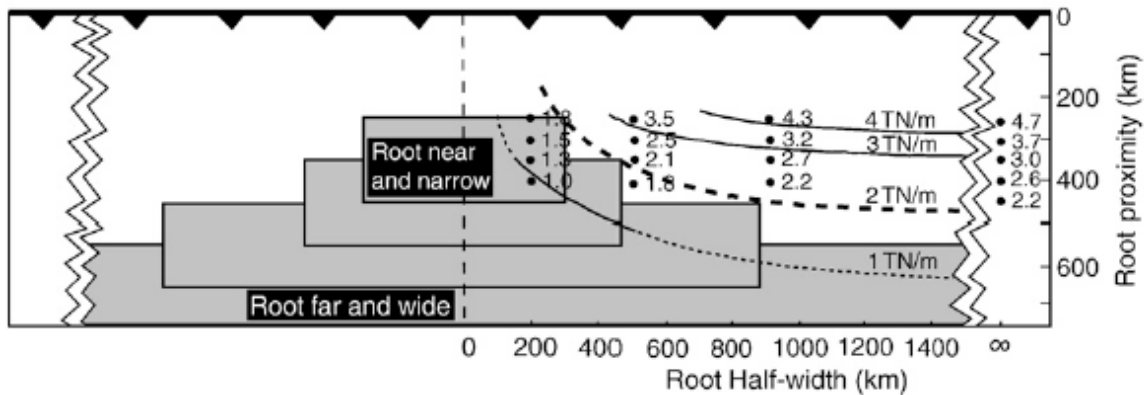
**Figure 2.8.** Mantle-wedge pressure and continental compression for models with roots of various along-strike widths, using the 3-D mesh shown in Fig. 2.7. The right side of the plot has a reflecting boundary condition, solid green line is for 200 km half-width root, long-dashed blue line for 500 km half-width, short-dashed red line for 900 km half-width (a) Mantle-wedge suction as a function of along-strike position, for a sample point in the center of the asthenosphere and 80 km to the right of the slab at this depth. (b) Compressive force (per meter of along-strike plate width) near the subduction zone in the continental plate, as a function of along-strike position.

Our modeling is consistent in that the pressure becomes spatially smoothed near the wedge tip when the viscosity is very low. Results for 2-D models are very similar to those run with very low asthenospheric viscosities in which the root penetrates the asthenosphere (Fig. 2.6): as discussed above, the asthenosphere confined to the mantle-wedge cavity maintains a near-uniform low pressure similar to that created with greater mantle viscosities.



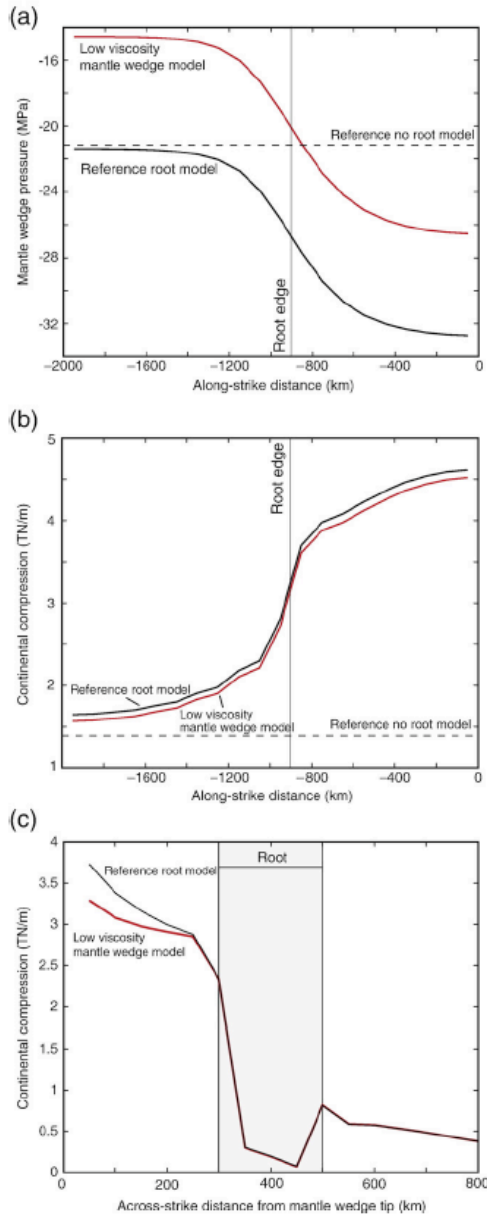
**Figure 2.9.** Effects on continental compression and mantle-wedge pressure caused by varying root width and location. (a) Continental compression as a function of root along-strike half-width for several root distances from the mantle wedge tip. (b) Mantle wedge pressure as a function of root along-strike half-width for several root distances from the mantle wedge tip. (c) Continental compression as a function of root distances from the mantle wedge tip for several root half-widths. (d) Mantle wedge pressure as a function of root distances from the mantle wedge tip for several root half-widths.

Figure 2.11 shows the effects of incorporating a very low viscosity mantle wedge tip in 3-D. For root half-width of 900 km, reducing the mantle wedge viscosity to  $10^{18}$  Pa·s (compared to  $5 \times 10^{19}$  Pa·s in our reference model) preserves the character of the



**Figure 2.10.** Amount of continental compression as a function of root along-strike half-width and root distance to the mantle wedge tip. Plot shows the amount of compression that is in addition to the 1.44 TN/m created by the rootless model. Labeled points show results of model runs.

mantle-wedge pressure variations along strike and reduces mantle wedge suction at our sample point (within the very low viscosity wedge) by about 7 MPa (~20% reduction) along the entire length of the subduction zone (Fig. 2.11a). The along-strike pressure drop is only marginally greater than our reference case (11.9 MPa compared to 11.3 MPa, Fig 2.11a). Continental compression is nearly unaffected by the presence of the very low viscosity channel, both in magnitude and in along-strike form (Fig 2.11b-c). This indicates that the effect of the very low viscosity wedge tip is confined to the region of the wedge tip; it may, however, have effects of subduction evolution that we have not modeled.



**Figure 2.11.** Effects on continental compression and mantle-wedge pressure caused by the inclusion of a very low viscosity mantle wedge tip. Low-viscosity prism represents the preferred model of Billen and Gurnis (2001). It has a viscosity of  $10^{18}$  Pa·s, extends to 250 km depth and 250 km away from the mantle wedge tip. Results from the low-viscosity wedge model (red) are compared with the reference model (Fig. 2.1). (a) Mantle wedge pressure as a function of along-strike distance, along a line at 150 km depth and 80 km horizontally away from the slab. This line is within the low viscosity prism. (b) Continental compression as a function of along-strike distance. (c) Continental compression as a function of across-strike distance.

### 3. DISCUSSION

#### 3.1. General Discussion

The increased suction in the mantle-wedge between the subducting slab and the root is fundamental to increasing continental compression and pulling the continent trenchward. Qualitatively, these effects behave in ways that are expected. Modeling quantifies the relative importance of these effects and their dependence on root geometry and other aspects of viscosity distribution.

Root width and distance from the wedge tip have important influence on the effects we model. If we consider 2 TN/m of continental compression to be a major effect, our models require a 1600-km-wide root that needs to be closer than ~400 km to the mantle wedge tip. As the root is moved farther away from the subduction zone, the dynamic effects of the root diminish rapidly. (For the trench-normal root cross section used in our study, shown in Fig. 1, the minimum distance between the slab and the root is ~100 km less than the distance between the root and the wedge tip, and it is the minimum distance that is thought to be most important in creating anomalous mantle-wedge suction.) Roots of finite width excite along-strike flow of asthenosphere toward the root center, where it is evacuated by slab subduction. The along-strike flow is a response to the greater mantle-wedge suction in the vicinity of the root. This effect is similar to that found by Kneller and van Keken (2008) for subducting slab that varies in dip angle along strike.

Inclusion of a very low viscosity mantle wedge tip extending to a depth of 250 km in our models does not have significant influence on the regional dynamics. This

behavior is similar to that found by Manea and Gurnis (2007), in which a very low viscosity wedge tip extending to 200 km depth evolves a slab dip profile and wedge pressure field that are similar to their model without the very low viscosity wedge tip. When they consider a deeper zone of very low viscosities, mantle-wedge suction diminishes in a manner similar to our models with a thick asthenosphere. In our models of instantaneous flow, the unimportance of a shallow wedge tip on regional dynamics occurs because two competing effects nearly cancel one another. A reduced suction in the low-viscosity wedge tip, by itself, would cause reduction in the suction in the asthenosphere between the root and the low-viscosity root tip. Compensating this is the effect of increased mantle flow up into the low viscosity wedge-tip region, which enhances flow-induced pressure drop in the asthenosphere adjacent to the root.

The increase in the magnitude of continental compression is an impressive  $\sim 4$  TN/m in our reference root model (Fig. 2.4b). Assuming local isostasy and a crust initially at sea level and 35 km thick, uplift of 3-4 km would be created by 4 TN/m of compression. In addition to compressing the continent, the mantle-wedge suction also pulls this portion of continent down. In our reference root model, the nearly uniform increase in downward pull of  $\sim 12$  MPa caused by the root-induced suction (Fig. 2.4a) is isostatically equivalent to depressing topography by nearly 400 m in the area between the subduction corner and the root. Including this amount of subsidence, our reference root model would result in  $\sim 3$  km of net uplift compared to the no-root reference model.

### 3.2. Influence of cratonic roots on flat-slab subduction

Subduction beneath continents tends to be shallower than that beneath ocean lithosphere by an average of  $\sim 20^\circ$  (Lallemand et al., 2005), and flat-slab subduction beneath ocean lithosphere is not observed. Also, a net westerly drift of plates relative to hotspots is recognized (e.g., Gripp and Gordon, 2002), which is commonly attributed to lateral viscosity variations, most notably deep continental roots (Ricard et al., 1991), especially in conjunction with a weak asthenosphere (Cadek and Fleitout, 2003). The specific cause of these behaviors is, we believe, the suction effects created by the cratonic roots. Because we have not modeled the time evolution of subduction, we cannot address if the slab lifting action of this suction is expected to cause flat-slab subduction. However, flat-slab subduction is not common beneath continents even when near a root, and hence the actual suction effects created by a root typically are insufficient to lift the slab completely against the overriding plate (van Hunen et al., 2004). The occurrence of flat subduction often is associated with ocean slab made buoyant by thick ocean crust, such as that carrying ocean plateaus (Livacari et al., 1981; Saleeby, 2003) or aseismic ridges (Gutscher et al., 2000). Even so, subduction of magmatically thickened crust is not observed to cause flat subduction beneath ocean lithosphere. Apparently, the buoyancy effects of thick crust alone are insufficient to cause flat-slab subduction, but rather the combined effects of buoyant slab and enhanced mantle-wedge suction, perhaps in conjunction with other processes, are required. This is supported by the current locations of Andean flat-slab subduction beneath southern Peru and northern Chile, corresponding

respectfully to the Juan Fernandez and Nazca aseismic ridges (e.g., Gutscher et al., 2000). Similarly, flat Laramide subduction is associated with subduction of an oceanic plateau (Saleeby, 2003) during a time when normal subduction occurred beneath Canada, where cratonic mantle root also is present.

When slab flattening occurs, highly compressive tectonics is observed. This often is viewed as a consequence of increased basal tractions that result from slab contact (e.g., Bird, 1988). Periods of flat-slab subduction also are times of unusually rapid trenchward continental motion, which is probably caused by an increase in mantle wedge suction. We expect this behavior to result from the narrowing of the mantle wedge and restriction of return flow pathways to replenish mantle being evacuated by subduction.

Flat-slab subduction beneath southern Mexico, where slab flattening has occurred without a nearby cratonic root, is an exception that suggests alternative conditions for slab flattening. Unlike other areas experiencing flat-slab subduction, the Mexican plate boundary is not compressional, indicating unexceptional mantle-wedge suction. Beneath Mexico, slab flattening may be related to a tear and detachment of the deeper slab that reduces the slab pull force (Kim et al., 2006; Ferrari, 2006). Also potentially important are the buoyancy contributions of young slab and the shallow depth of the ocean crust (at only ~50 km depth, Manea et al., 2006) beneath Mexico, probably causing the crust to remain unaltered to eclogite (Gutscher et al., 2000).

We have focused on the effects of mantle wedge suction in compressing the continent and pulling the continental plate trenchward. The suction effect would also

be expected to contribute to the convergent velocity of the subducting plate by pulling the slab forward (to the right in Figs. 2.2 and 2.5). Hence, root-enhanced suction may contribute to rapid subduction by drawing both plates toward each other.

### 3.3. Modeling limits

Many subduction parameters are significant to the subduction process (e.g., Lallemand et al., 2005). Our investigation has focused only on the effects of a cratonic root near the subduction zone, and even then only in instantaneous modeling.

We have not modeled the increase in speed of the overriding continental plate, which we have held fixed at the subduction zone. We infer that the continent would accelerate in response to the force applied to this plate (Fig. 2.3b), which is large compared to typical levels of applied force of a few TN/m (Bird, 1998; Humphreys and Coblenz, 2007). However, we have not addressed how the additional force is balanced by forces that depend on plate or subduction velocity, such as more rapid plate motion over the underlying mantle and moving the subducting plate out of the way as the continent overrides the subduction zone. Other authors have considered this topic (e.g., Arcay et al., 2008)

Asthenospheric viscosity as a function of depth is not well resolved, and root suck is most effective when the root penetrates the asthenosphere. If the base of the asthenosphere is gradual, then the root must penetrate to significantly higher viscosities. If root suction is the process responsible for intense subduction-related orogeny and rapid plate motion, then our modeling suggests that the asthenosphere is

a thin, weak layer beneath plates (Phipps-Morgan et al., 1995; Toomey et al., 2002) through which major cratonic roots penetrate (Humphreys and Coblenz, 2007).

Although we have modeled the 3-D effects of a finite-width root, we have not modeled the 3-D effects of flow around sides of a finite-width slab. The modeling of finite-width slabs (Stegman et al., 2006; Schellart et al., 2006; Piromallo et al., 2006) offers guidance in assessing this effect. When the slab edge is near, toroidal flow around the edge of the slab supplies asthenosphere into the mantle wedge and the suction effects diminish owing to the relatively easy supply of asthenosphere. This effect reduces mantle-wedge pressure significantly within a few hundred km from the slab edge, which is a similar scale of effect to that described above for finite-width roots.

#### 4. CONCLUSIONS

We model the decrease of mantle wedge pressure resulting from inhibited corner flow affected by deep cratonic roots. This suction acts to pull the continental root towards the subduction zone with a force that depends on root width and upper mantle viscosity; for reasonable values, we obtain a force of  $3\text{-}5 \times 10^{12}$  N/m (enough to support  $\sim 3\text{-}4$  km of elevation). This force places the intervening continental lithosphere in strong compression, favors the lifting of the subducting slab, and supplies a large trenchward-directed force on the continental plate. This may account for the highly compressive Laramide and Andean orogenies that each occurred during times of relatively rapid trenchward motion of the continental plate. Without the root

suck mechanism, the relationship between compression and acceleration of the continent is otherwise difficult to explain. This suction also would be expected to enhance the ocean plate convergence speed, and pull the continental margin down  $\sim 0.5$  km. Root-induced suction is most effective when the root penetrates through the asthenosphere and into the mesosphere, and the root needs to be closer to the mantle wedge tip than  $\sim 400$  km. A root of finite width (in the trench strike direction) reduces the intensity of these effects by a factor of  $\sim 2$  within  $\sim 200$ - $300$  km of the root edges.

## CHAPTER III

### NAZCA-SOUTH AMERICA INTERACTIONS AND THE LATE EOCENE-LATE OLIGOCENE FLAT-SLAB EPISODE IN THE CENTRAL ANDES

Reproduced with permission from Richards, M.; Humphreys, E.; *Tectonics*, **2012**, 31, *TC2013*. Copyright 2012, American Geophysical Union.

#### 1. INTRODUCTION AND BACKGROUND

The localization in space and time of early (~50-40 Ma) tectonism in the Central Andes must be considered when evaluating the subsequent regional evolution. Proposed models have suggested that an abrupt acceleration in relative motion between the Farallon/Nazca plate and the South American plate at ~30 Ma may have led to compression of the continent [Russo and Silver, 1994; Silver *et al.*, 1998]. It appears that this relative motion change occurred at ~25-24 Ma [Tebbens and Cande, 1997; Somoza 1998], when westward acceleration of South America also began. We propose an alternative model to explain strong compression of the Central Andean margin and coincident flat-slab formation during late Eocene to late Oligocene while reconciling relative plate motions, intense forearc shortening that predates 25 Ma [Arriagada *et al.*, 1998], and the location of thick craton-bearing lithosphere. Flat-slab geometry has been proposed for this period in Peru and Bolivia [Isaaks, 1988; James and Sacks, 1999], but the dynamic driving force has yet to be examined. We argue for the importance of the interaction between the South American cratonic lithosphere structure and the down-going Nazca plate, and extend the modeling of O'Driscoll *et al.* [2009] to demonstrate the role of enhanced mantle wedge suction in Eocene and Oligocene Andean tectonics.

## 1.1. Andean Orogeny

The orogenesis that built the high-standing Andean tectonic belt occurred over the past 70 m.y. [e.g. *Coney and Evenchick, 1994; Sempere et al., 1997; Horton et al., 2001; McQuarrie et al., 2005*], and the western South American margin has been in a state of compression since at least the early Paleocene. The modern ocean-continent convergent Andean plate boundary is commonly compared to the Sevier and Laramide orogenies of North America. There has been along-strike heterogeneity throughout the Cenozoic, expressed as variations in slab geometry, arc activity, composition of the down-going slab and shortening of the western margin along strike. Recently, *Capitanio et al. [1999]* modeled subduction dynamics related to the variation in continental and lithospheric thickness across the South American margin for the Cenozoic era, finding an important correlation between thickness of the oceanic and continental plates with construction of the Altiplano and Puna plateaus, as well as development of the Bolivian Orocline curvature.

During the late Eocene and into the Oligocene, flat-slab subduction is thought to have occurred beneath the southern Peruvian and Bolivian Central Andes [*Isacks, 1988; James and Sacks, 1999*], and a younger (~18-12 Ma) flat-slab is proposed for the Miocene beneath the Puna Plateau [*Kay and Abbruzzi, 1996; Kay et al., 1999*]. *Isacks [1988]* was the first to suggest flat-slab formation beneath the Altiplano between ~38-25 Ma. Further support for a flat-slab include a lull in volcanic arc activity by *Lamb and Hoke [1997]*, a broadening of the arc in Peru [*Mamani et al., 2010*], and forearc shortening in Peru and northern Chile with an inboard jump in shortening at 40 Ma

[*McQuarrie et al.*, 2005]. *Martinod et al.* [2010] may be the first to suggest a link between flat-slab behavior and the formation of the Bolivian Orocline (Figure 3.1) during the early stages of the Altiplano uplift. Here, we present a model that addresses the timing of the formation of the Bolivian Orocline in conjunction with dynamically evolving subduction regimes that operated throughout the Cenozoic. We find that phases of slab flattening and steepening exerted a primary control on arc magmatism and regional crustal shortening. Our model is guided by the history of shortening and rotational strain presented by *McQuarrie et al.* [2005] and *Arriagada et al.* [2008].

## 1.2. Plate motion history

The plate circuit through the Pacific-Nazca-Antarctic-Africa-South American plates has been used to calculate Nazca (Farallon)-South America relative velocity [*Pilger*, 1983, *Pardo-Casas and Molnar*, 1987; *Tebbens and Cande*, 1997; *Somoza*, 1998]. The primary features of these models are episodes of fast and slow convergence during the Cenozoic [*Pardo-Casas and Molnar*, 1987], strong changes in the obliquity of convergence and along-strike variation in trench velocity [*Somoza*, 1998], and a plate boundary reorganization at ~25 Ma that includes a change from a NE subducting Farallon plate to more easterly subducting of Nazca plate [*Tebbens and Cande*, 1997]. The plate motion reconstruction software *Gplates* [*Boyden et al.*, 2011] utilizes the stage poles of these authors and the continuously closed plate algorithm of *Gurnis et al.* [2011], providing a useful tool to investigate plate reconstruction hypotheses.

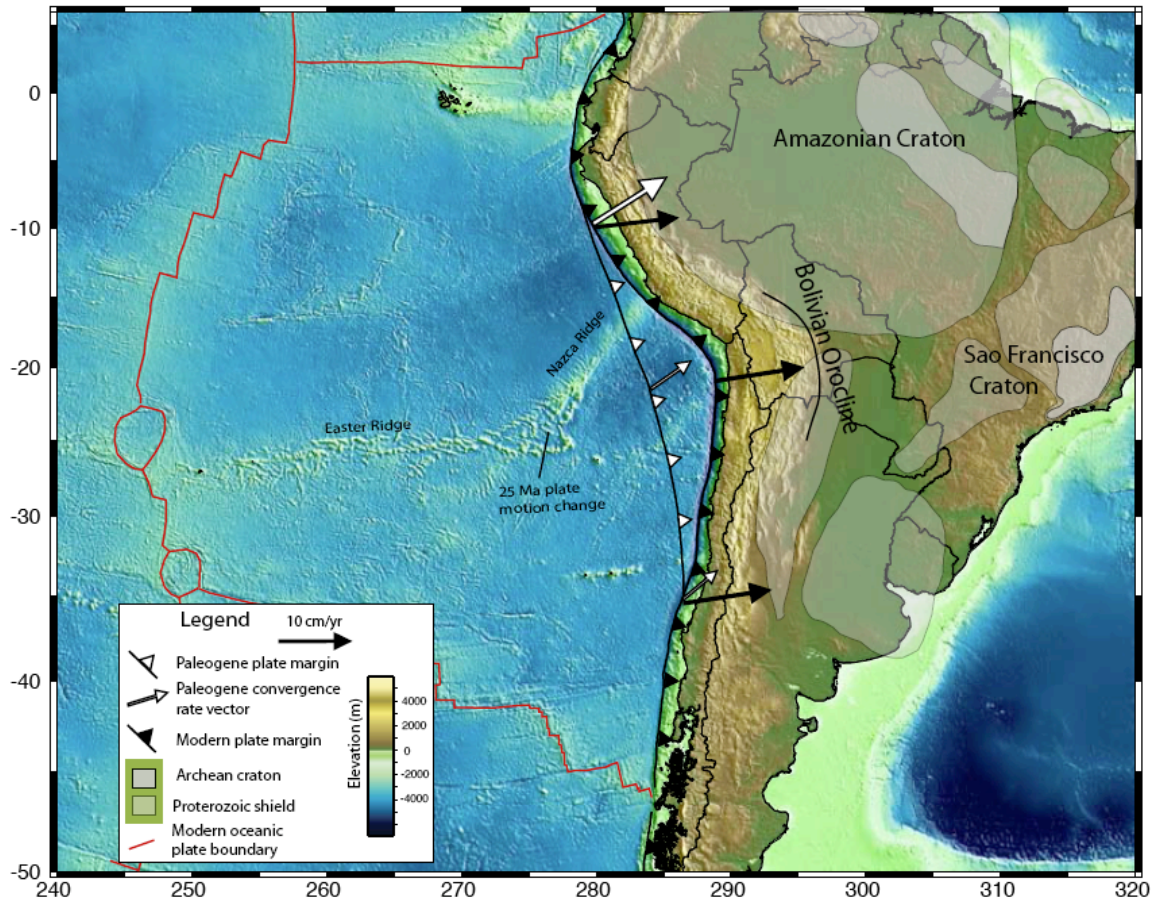


**Figure 3.1.** Tectonic map of South America. The Archean and Proterozoic craton/shield structure is based on surface exposure, taken from *Fuck et al.* [2008], is shown in light grey and grey, respectively. Trench geometry and convergence vectors are given for the modern and pre-Miocene configurations in black and white, respectively. The Easter-Nazca ridge bend is evidence for the 25 Ma Nazca plate motion change. The Bolivian Orocline is outlined across the Central Andes.

The relative motion between Africa and South America has been used to infer the onset of strongly compressive deformation in the Central Andes [*Silver et al.*, 1998].

*Russo and Silver* [1996] use the 30 Ma timing of westward acceleration of South America reported by *O'Connor and Duncan* [1990] to explain the development of trench parallel mantle flow inferred from SKS splitting results [*Russo and Silver*, 1994]. This timing of South American westward motion is linked to the slowing of Africa's northward absolute

velocity, and is an important point within the conceptual model of *Silver et al.* [1998]. More recently, the timing of Africa's northward slowing was more accurately resolved to be ~25 Ma after consideration of more Atlantic isochron data, timing of Red Sea opening and shortening constraints in Iran [*McQuarrie et al.*, 2003]. We discuss the consequences of this adjustment in timing in section 3.

### 1.3. Mechanisms of developing flat-slab subduction

Numerous mechanisms have been proposed to explain slab flattening, such as subduction of buoyant oceanic plateaus, enhanced overriding of the upper plate in the mantle reference frame, and mantle wedge suction force [*Stevenson and Turner*, 1977; *Tovish et al.*, 1978; *van Hunen et al.*, 2004]. Dynamic effects of positive slab buoyancy are required to overcome slab-pull to induce flat-slab formation. The subduction of oceanic plateaus has been cited as an important factor in developing a flat subduction angle, with the modern Peruvian flat-slab segment being a type example [*Gutscher et al.*, 1999]. Upon subduction of an oceanic plateau, thick basaltic crust and underlying harzburgite mantle are less dense than the surrounding mantle, and contribute to slab flattening [*van Hunen et al.*, 2002]. Also, trenchward motion of the overriding plate can displace the down-going slab, thereby enhancing flattening behavior [*Vlaar*, 1983; *van Hunen et al.*, 2000]. Another slab-lifting mechanism is mantle wedge suction force [*Stevenson and Turner*, 1977; *Tovish et al.*, 1978], which can be enhanced by subduction near a thick, cratonic root [*O'Driscoll et al.*, 2009]. It appears that all three of these mechanisms may have contributed to flat-slab formation beneath the South American

margin during various periods, although their relative importance is not well understood and are variable with time and location.

We consider the tectonic evolution of the late Eocene to late Oligocene Central Andes based on slab-craton interaction and buoyant plateau subduction. We conclude that (1) there was a direct relationship between the plate convergence directions and the location of cratonic root positions that led to a flat-slab episode which was coeval with the formation of the Bolivian Orocline curvature prior to 25 Ma, and that (2) the slab flattening process was aided by subduction of buoyant lithosphere.

## 2. CENTRAL ANDEAN TECTONICS AND THE INFLUENCE OF SOUTH AMERICAN CRATONS

### 2.1. South American shield and cratons

A large portion of South America is composed primarily of Proterozoic and older cratons with accreted Phanerozoic terranes along the western margin. Figure 3.1 shows the distribution of the cores of cratons composed of rocks of Archean (white) and Proterozoic (light white) ages inherited from the Rodinian Supercontinent [Fück *et al.*, 2008]. The Amazonian Craton (AC) in NE Brazil is Archean to middle Proterozoic [e.g. Schobbenhaus *et al.*, 2004]. These ancient bodies are imaged by surface wave tomography to a depth of 200 km, possibly being as deep as 250 km in the Archean portions [Heintz *et al.*, 2005]. The depths to the base of these cratons are unclear due to the depth uncertainty that arises from surface wave tomography imaging. Artemieva and Mooney [2001] showed that Archean cratonic bodies are generally thicker than younger cratonic bodies (250 vs. 200 km thick, global average), and we use this relationship when

considering lithospheric thickness in our modeling, along with results from tomographic imaging. The fast seismic anomalies presented in *Heintz et al.* [2005] are in agreement with this our modeled craton thickness.

The largest mass of the cratonic area of South America is centered in Brazil, although the Archean Sao Francisco Craton (SFC) extends south into Uruguay [*Fuck et al.*, 2008]. Both appear to be deep enough to cause enhanced mantle wedge suction during subduction [*O'Driscoll et al.*, 2009]. There are younger Precambrian rocks that flank the older craton and are present beneath the eastern Andes and have been underthrust beneath the Altiplano [*McQuarrie et al.*, 2005], however, large portions of these rocks are covered by sediments between outcrops in the cratonic cores in the east and basement rocks involved in deep-seated thrust faults to the west. We consider the western extent of deep (>60 km) elastic thickness determined by *Pérez-Gussinyé et al.* [2008] to delimit the extent of cratonic extent. Based on the seismic images, lateral elastic thickness variation, surface exposure, and assuming the position of the Eocene mantle wedge tip, distances from the estimated mantle wedge tip to the adjacent craton for the AC and SFC are 350 and 650 km, respectively (these values used in modeling in section 3.2.2). Further development of these modeling parameterization is discussed below.

## 2.2. Central Andean (10°-30° S) episodes of flat-slab subduction

Transitions in subduction from normal to flat and flat to normal are inferred from the geologic record [e.g. *Ramos and Folguera*, 2009]. During flattening, the volcanic front migrates into the backarc region as the arc expands its spatial extent as the down-

going slab approaches the base of the continental lithosphere. Greater coupling occurs between plates, and foreland deformation and loading commences as a landward advancing thrust front with related foreland basin subsidence. As normal-angle subduction is re-established and the slab steepens, a major pulse of mafic volcanics occurs, with rhyolitic magmas sourced from crustal melting [*Hoke et al.*, 1994]. Based on these criteria, nearly the entire Andean margin has been subjected to shallow angle subduction during the Cenozoic [e.g. *Ramos and Folguera*, 2009]. Two prominent flat-slab segments are currently active: The central Chilean (or Pampean), and Peruvian segments. Using intraslab seismicity, *Barazangi and Isacks* [1976] first identified the flat geometry of portions of the modern Nazca slab that subducts beneath between Peru and central Chile. The two regions underlain by flat-slabs also exhibit gaps in the magmatic activity [e.g. *Cahill and Isacks*, 1992]. Based on the onset time of magmatic quiescence, the Peruvian flat-slab is thought to have been established at ~11 Ma [*Ramos and Folguera*, 2009], and the Pampean slab flattened at ~12 Ma [*Kay et al.*, 1987].

The Central Andean margin of southern Peru and Bolivia is thought to have experienced a prolonged period of flat-slab subduction during the late Eocene through late Oligocene, suggested from a lull in volcanic arc activity between 40-25 Ma [*Bissig et al.*, 2008; *James and Sacks*, 1999]. Cessation of arc magmatism migrated from central Peru southward through Chile and Bolivia, consistent with a diachronous flattening progression. *Bissig et al.* [2008] describe broadening of the Peruvian arc in the late Eocene to early Oligocene (42-37 Ma), and *Mamani et al.* [2010] show an eastward sweep of southern Peruvian and north Chilean arc volcanics, constraining the start of the flat-slab period to 35 Ma. Interpreting similar behavior, *Kay et al.* [1999] describe 18-12

Ma slab shallowing beneath the southern Altiplano and Puna plateaus. This segment has an along-strike position between the 37-25 Ma Central Andean flat segment and the modern Pampean segment.

While slab flattening appears to be a common occurrence beneath South America, the underlying cause(s) of this activity may be variable through time. Of the factors mentioned in section 1.3, only enhanced suction above the slab is a common contributor. Continental overriding appears to have occurred after ~25 Ma [*Somoza, 1998*], and subduction of buoyant lithosphere cannot be confidently identified as a contributing factor in all cases. Apparently, a combination of factors is required to reduce the subduction angle and obtain flat-slab subduction.

### 2.3. The Andean Orogenies in the Cenozoic

We suggest four distinct periods of Andean deformation and link these periods to geometry, direction, velocity of the subducting Nazca plate, and the lithospheric structure of the interior South American plate. Our model focuses on the Central Andean (~15-25° S) flat-slab episode that occurred at ~35-25 Ma (Figure 3.2). Previous models of shortening regimes [*McQuarrie et al., 2005; Arriagada et al., 2008*] and characterization of Andean flat-slab episodes [*James and Sacks, 1999; Ramos and Folguera, 2009*] guide our tectonic model. We incorporate various stages of plate motion, shortening, slab behavior, and volcanism related to the geologic and geodynamic evolution of the Central Andes and the Bolivian Orocline.

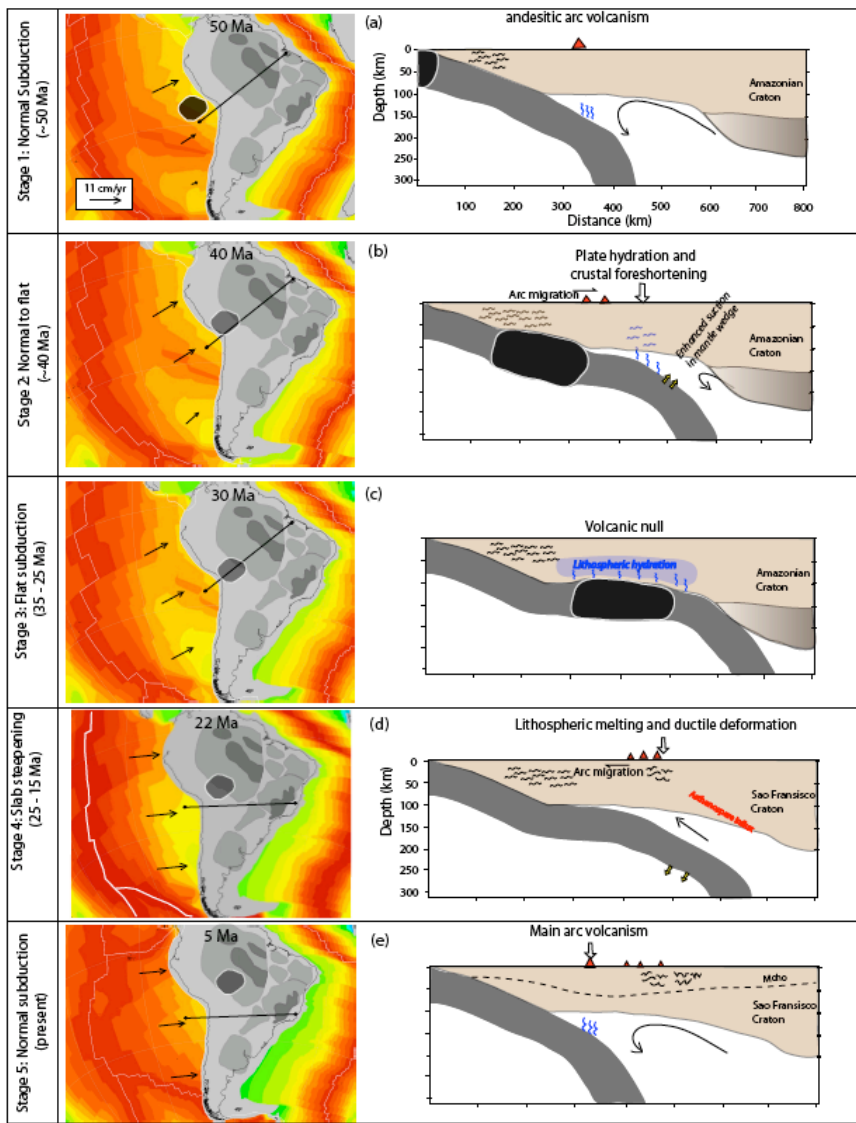


**Figure 3.2.** Summary of tectonic model, modified from *James and Sacks* [1999]. (a) Stage 1, Eocene configuration, continuous subduction beneath entire margin with faster convergence to the north. Normal arc volcanism present. The slab beneath the Central Andes is aligned down-dip with the Amazonian Craton. (b) Stage 2, onset of plateau subduction and beginning of strong forearc shortening. Arc volcanism rapidly migrates landward as slab angle begins to flatten. (c) Stage 3, Flat-slab subduction occurs as the Bolivian Orocline is fully developed. Arc volcanism ceases as the slab approaches and hydrates the base of the continental lithosphere. (d) Stage 4, Nazca slab steepens along with a strong decrease in subduction obliquity. The slab beneath the Central Andes is now aligned with the Sao Francisco Craton. Hot asthenosphere flows into the mantle wedge, producing voluminous melting. Shortening is focused in the Eastern Cordillera. (e) Eastward-directed subduction commenced as shortening is focused further eastward in the Interandean and Subandean belts.

### 2.3.1. Onset of a compressional margin

*Pardo-Casas and Molnar* [1987] showed that the Andean trench velocity was weakly convergent to divergent throughout the Mesozoic and into the Eocene (Figure 3.2a). Abundant arc volcanism occurred as calc-alkaline magmatism along the western Cordillera [*Pichowiak et al.*, 1990; *Haschke et al.*, 2002], as well as the emplacement of the 100-55 Ma Coastal Batholith in Peru [*Atherton*, 1990]. Plate reconstructions [*Pilger*, 1983; *Pardo-Casas and Molnar*, 1987; *Tebbens and Cande*, 1997; *Somoza*, 1998] of the Mesozoic and early Cenozoic include the Phoenix Plate as part of a ridge-ridge-ridge triple junction with the Pacific and Farallon Plates [*McCarron and Larter*, 1998].

Based on preserved synorogenic sediments in the Altiplano, *McQuarrie et al.* [2005] proposed that initial mountain building began around 70 Ma in the Bolivian Andes. During the Paleocene to mid-Eocene (~70-50 Ma), convergence velocity varied greatly along strike of the margin, with convergence rates of ~50 mm/yr in the northern latitudes decreasing to small (perhaps negative) values in the south [*Pardo-Casas and Molnar*, 1987]. Between ~50-37 Ma, an increase in the convergence rate occurred along the entire margin [*Pardo-Casas and Molnar*, 1987], coincident with the onset of flat-slab development and a major shift in deformation from the western Cordillera to the eastern Cordillera [*McQuarrie et al.*, 2005].

### 2.3.2. Flat-slab period in the Central Andes, Peru and Bolivia

The period 37-25 Ma appears to have had both flat-slab subduction in the Central Andes and rapid slowing of convergence (< 50 mm/yr) that occurred along the entire

margin [*Martinod et al.*, 2010; *Pardo-Casas and Molnar*, 1987; *Somoza*, 1998]. This flat-slab episode (Figure 3.2b-c) is inferred from a magmatic lull [*James and Sacks*, 1999], which coincided with the simultaneous development of Bolivian Orocline curvature [*Arriagada et al.*, 2008]. *Mamani et al.* [2010] indicate a widening of the volcanic arc in southern Peru starting at 45 Ma. Arc activity shut off above the flat-slab, first in Peru, then Bolivia and Chile, diachronously flattening from north to south [*Bissig et al.*, 2008; *Lahsen*, 1982]. *Arriagada et al.* [2008] suggested that the western margin of South America was nearly straight prior to the onset of shortening and block rotation that has resulted in the present-day Bolivian Orocline. Analysis of paleomagnetically determined forearc block rotation of crust within the Bolivian Orocline and balanced cross section determination of shortening has clarified the timing of the Paleogene deformational history during 45-20 Ma [*McQuarrie*, 2002; *Roperch et al.*, 2006; *Arriagada et al.*, 2008; *Gotberg et al.*, 2010]. Previous attempts to reconstruct the Andean margin that focus on the most recent 20-15 m.y. do not account for pre-Miocene shortening and crustal rotation [e.g. *Barke et al.*, 2007]. While the importance of the Eocene and Oligocene shortening is emerging as a major factor in the greater evolution of the Andean Orogeny, the compression and crustal shortening associated with this time has only recently been linked to the flat-slab regime that drove the formation the Bolivian Orocline [*Martinod et al.*, 2010].

### 2.3.3. Re-steepening of the slab

At the end of the flat-slab episode, a change in subduction obliquity occurred, marked by a strong change from dextral to normal convergence in the Central Andes of

Chile and southern Peru [Somoza, 1998]. Reorganization of the Pacific-Antarctica-Nazca triple junction occurred between 25-23 Ma, inferred via a northward jump of ~500 km [Tebbens and Cande, 1997]. As a result, Nazca-Antarctic spreading rotated ~40° clockwise and the Nazca Plate accelerated eastward. The convergence between the Nazca and South American Plates increased at ~25 Ma to 15 cm/yr [Somoza, 1998]. With this new convergence configuration, the Central Andes were situated between the trench and the distal, Sao Francisco Craton (compare azimuth of cross section between Figure 3.2a-c and Figure 3.2d-e).

Volcanic activity may signal that the slab dip angle returned to a moderate dip, assuming that recurrence of arc activity following a volcanic lull is indicative of such a change. A diachronous variation between Peruvian and Bolivian arc activity is observed during the proposed slab steepening period. *Mamani et al.* [2010] show arc activity migrated toward the trench between 30-25 Ma, whereas *Gillis et al.* [2006] report 25 Ma volcanism at the Quimsa Cruz Batholith in the Eastern Cordillera. Arc activity was re-established in the newly formed Altiplano in the east, migrating to the west until occupying roughly what is now the Central Volcanic Zone [Figure 3.2d, *Hammerschmidt et al.*, 1992]. The initial phase of melting began at 25 Ma as a wide range of alkalic mafic to felsic volcanics [e.g. *Avila-Salinas*, 1991], and east to west migration ceased between 20-15 Ma [*Hammerschmidt et al.*, 1992].

#### 2.3.4. Development of the modern Andean system

*James and Sacks* [1999] proposed that the lithosphere was weakened by post-hydration magmatism, which guided subsequent deformation and uplift of the Altiplano.

The post 25 Ma shortening history is consistent with the proposal of *James and Sacks* [1999], where shortening has been focused east of the Andean Plateau. *Oncken et al.* [2006] provide a post 25 Ma shortening history, indicating that deformation took place in the Eastern Cordillera and Interandean belts between 25 and ~11 Ma, gradually shifting eastward to the Subandean belt after 11 Ma. Alternatively, the Eastern Cordillera and Interandean zone may have been active until 20 Ma, with shortening along the Subandean zone beginning as early as 18-15 Ma [*McQuarrie et al.*, 2005; *McQuarrie et al.*, 2008; *Barnes et al.*, 2008]. This eastward expansion of shortening began to incorporate greater amounts of underthrusting of Proterozoic Amazonian shield lithosphere beneath the Altiplano, as suggested by *McQuarrie et al.* [2005] who preferred convective removal of Andean lithosphere at 25 Ma beneath the Altiplano to both account for lithospheric thickening and to allow the necessary space for shield underthrusting. Evidence for delamination of continental lithosphere may also be provided by a pulse of mafic volcanism in the Eastern Cordillera at 24-23 Ma [*Lamb and Hoke*, 1997].

The Miocene to modern Andes has seen formation of three flat-slab segments, the two modern sections in Peru and central Chile and the Puna segment between 18-12 Ma [*Ramos and Folguera*, 2009]. Late Miocene shallowing of the Nazca slab beneath Peru and central Chile led to the modern configuration of the Nazca slab, as imaged via earthquake hypocenter locations [*Barazangi and Isacks*, 1976; *Cahill and Isacks*, 1992]. The Peruvian slab is commonly cited as “type example” of flat-slab formation linked to the subduction of buoyant oceanic lithosphere [see *Gutscher et al.*, 1999 for further discussion].

*Kay et al.* [1999] summarized the Puna flat-slab episode, suggesting an analogy to the Central Andean episode described above and by *James and Sacks* [1999]. These modern phases of flat-slab geometry provide an analog to the processes that occurred during establishment of the 37-25 Ma Central Andean flat-slab, such as the geochemical evolution of volcanics that were sourced from varying crustal depths [*Kay et al.*, 1999] and broadening of the zone of compression/shortening above the central Chilean flat-slab, evidenced by basement-cored uplifts actively growing in the Argentinian Sierra Pampeana province [*Ramos et al.*, 2002].

### 3. GEODYNAMIC FORCES

We focus on the dynamic factors that may have given rise to both shallowing and steepening of the proposed late Eocene-late Oligocene flat-slab in the Central Andes. Previous studies have compiled evidence for the possibility of a flat-slab period during this time [e.g. *Sandeman et al.*, 1995; *James and Sacks*, 1999], and we offer the first dynamic mechanism(s) for this suggested slab behavior. Further, we consider the source of strong compression of the Peruvian, Bolivian, and northern Chilean Andes prior to ~45-25 Ma that was coincident with the timing of the Bolivian Orocline formation [*Arriagada et al.*, 2008]. The factors we present below relate to interaction between the down-going Nazca plate and the South American continent.

#### 3.1. “Stagnation point” conceptual model

A widely cited explanation for mid-Cenozoic to recent Andean tectonism is the “stagnation point” model of *Russo and Silver* [1994; 1996]. This model is motivated by

the observation of a mantle shear-wave splitting pattern that shows fast axis directions that are parallel to the strike of the Andean margin, and hence the inference of mantle flow above the Nazca slab. *Silver et al.* [1998] further developed this concept by arguing that roll-back of the Nazca slab beneath the Central Andes was incapable of keeping up with the onset of accelerated westward motion of South America, which they understood to have begun at ~30 Ma [*O'Connor and Duncan*, 1990]. They argued difficulty in evacuating the mantle wedge with horizontal flow away from a stagnation point beneath the Central Andes, thereby limiting slab retreat and forcing the local plate boundary into compression along the leading edge of South America. This conceptual model for the timing and location of Andean compression has guided subsequent modeling of the Andean Orogeny [e.g., *Sobolev and Babeyko*, 2005].

*Silver et al.* [1998] attribute westward acceleration of South America to an increase in net basal traction on South America caused by the ~30 Ma reconfiguration of mantle flow. A westward mantle flow is thought to result from a slowing of Africa as it collided with Eurasia (in an absolute plate motion reference frame) during roughly constant South Atlantic spreading. Modeling of the 1.5 cm/yr decrease of Africa's northeasterly motion shows a modest 0.5-1.0 cm/yr increase in South America's westward motion. *Silver et al.* [1998] suggest that this acceleration was the cause of compression and uplift of the Altiplano and development of the Bolivian Orocline, although a quantitative model for these forces was not developed.

While this model is relevant for Miocene and younger Andean orogenesis, it does not apply to the late Eocene and Oligocene history in the Central Andes. Africa's northward velocity slowed at ~25 Ma [*McQuarrie et al.*, 2003] and *Somoza* [1998] shows

that acceleration of the SA/Nazca convergence rate occurred at about 24 Ma, while it is clear that much of the forearc shortening responsible for development of the Bolivian Orocline occurred prior to the acceleration of SA/Nazca subduction. Figure 3.3 shows the results of *Arriagada et al.* [2008] for the history of shortening strain across the central Andes, based mainly on an extensive data set of paleomagnetic block rotations. Although better resolution of the history of strain in the time period ~15-30 Ma is needed, the majority of block rotation and shortening likely occurred prior to the acceleration in convergence rate at ~24 Ma [*Cesar Arriagada, personal communication*].

Although it seems quite plausible that trench-parallel flow may be occurring due to mantle resistance to slab rollback, as perhaps demonstrated by the shear wave splitting results, this resistance was likely not the agent responsible for the main portion of the 37-25 Ma Central Andean tectonism and the development of the Bolivian Orocline. As outlined above, there have been a number of flat-slab episodes along the Andean margin, which do not seem causally related to accelerated convergence (they are more commonly coincident with decelerated convergence). In fact, the proposed flat-slab regime that we are linking to the development of the Bolivian Orocline appears to have ceased at about the time of accelerated convergence. We therefore propose that another model, based more on “local” forces associated with the character of both the subducting and overriding lithosphere is needed, as outlined below.

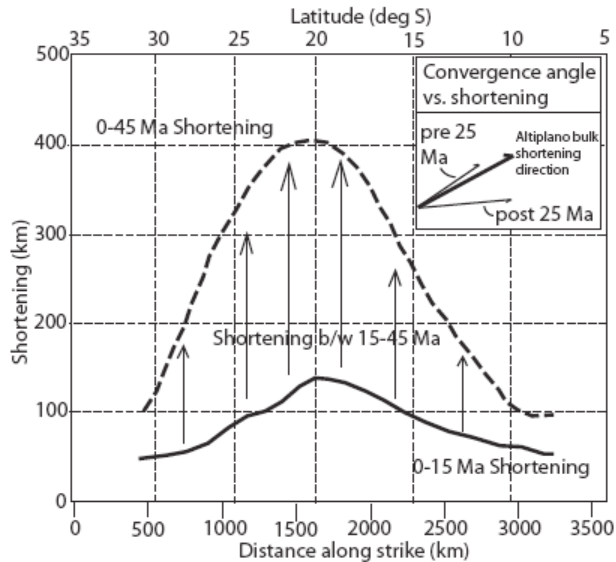


**Figure 3.3.** Timing of along-strike strain distribution across the central Andes, modified from *Arriagada et al.* [2008]. Results of 2-stage finite strain modeling, 0-15 Ma (solid line) indicates some focusing of strain in central Andes. Combined shortening from 0-45 Ma reveals strong along-strike gradient in shortening that created Bolivian Orocline curvature. This strain history indicates a strong degree of shortening between 15-45 Ma (arrows), where a significant portion is attributed to pre-25 Ma convergence. (inset) Comparison between pre- and post- 25 Ma convergence directions [*Arriagada et al.*, 2008, figure 6b] and the modeled forearc displacement field (bold). Significant shortening prior to 25 Ma plate motion change is inferred based on the sub-parallel orientation between the pre-25 Ma convergence vector and the average displacement direction of the shortening model.

### 3.2. Root suction model

#### 3.2.1. Summary of the cratonic root-enhanced suction mechanism

The deep lithospheric structure of the upper plate plays an important role within a subduction system, as evidenced by an average slab dip beneath continents that is  $\sim 20^\circ$  shallower than those beneath oceanic upper plates [*Lallemand et al.*, 2005]. In a subduction corner-flow system, the volume of mantle evacuated with the down-going slab must be replaced by mantle sourced from either beneath the overriding plate or around a lateral edge of the slab. Negative pressure in the mantle wedge is strongest in

the absence of nearby slab edges, where simple 2D corner flow (also known as poloidal flow) is dominant [Stevenson and Turner, 1977; Tovich *et al.*, 1978]. The presence of a deep lithospheric root restricts the supply of low-viscosity asthenosphere into the mantle wedge in this configuration.

*O'Driscoll et al.* [2009] analyzed this subduction scenario by developing a finite element model of a slab subducting beneath a continent that bears a cratonic root. This model quantifies dynamic forces associated with the inhibition of flow into the mantle wedge. Below, we extend this modeling by simulating subduction beneath a representative continental lithosphere for South America (Figure 3.4). Mantle entrained with the down-going slab must be replaced into the mantle wedge, and as the supply of mantle becomes inhibited, suction increases. Modeling shows that when a cratonic root inhibits slab-driven corner flow, the resulting pressure reduction creates a strong trenchward pull on the overriding continent and generates a slab lifting force. For instance, a 250 km deep, infinite-width root that lies 300 km from the mantle-wedge corner produces a two-fold increase in mantle-wedge suction and nearly a four-fold increase in continental compression compared to a rootless reference model (attaining up to 4 TN/m of lithospheric compression). When finite-width roots are wider than the distance to the mantle-wedge corner and closer than 400 km between the mantle wedge tip and cratonic root edge, compression of the continent between the root and the subduction zone is >50% that found in the infinite width root. North and South America are candidates for the application of root-enhanced suction. In North America, dynamic forces related to root-enhanced suction likely affected the Sevier [*Jones et al.*, 2011] and/or Laramide orogenies [*O'Driscoll et al.*, 2009].

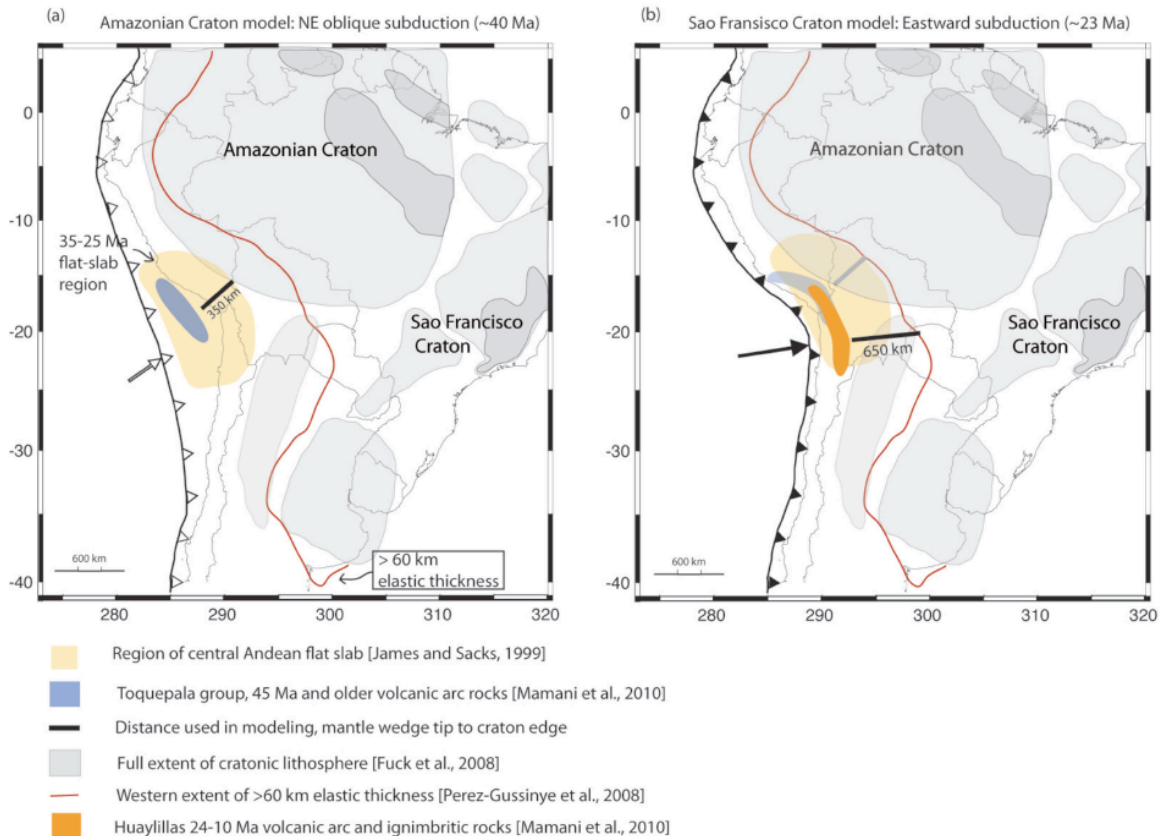


**Figure 3.4.** Summary of spatial scaling for modeled mantle wedge tip to craton edge distances. (a) Reconstruction of ~40 Ma lithospheric configuration. The location of pre 45 Ma volcanic arc rocks (blue) marks the approximate mantle wedge tip. The craton edge is marked by the edge of surface exposure of cratonic rocks [Fuck *et al.*, 2008]. The black line denotes the modeled distance of 350 km. In the supplementary content, we extend this line to the present western edge of >60 km elastic thickness [Pérez-Gussinyé *et al.*, 2008], giving a modeled distance of 650 km. (b) Reconstruction of ~23 Ma lithospheric configuration. The simplified location of 24-10 Ma arc rocks (orange) gives the approximate wedge tip. The eastern craton edge is approximated by the location of >60 km elastic thickness. We also model a 1250 km offset, using the edge of the Sao Francisco Craton in Brazil.

Subduction beneath the southwest North American margin was aligned with the Canadian Shield (i.e., the subduction zone was approximately parallel to the southwestern margin of the Canadian Shield). North of the main Laramide activity, the Kula-Farallon slab window was present within the slab beneath the northern U.S. or southern Canada [Breitsprecher *et al.*, 2003], allowing mantle to be supplied to the corner-flow from

beneath the slab, thereby minimizing enhanced suction effects. Further south, the slab was continuous along-strike, requiring the supply of mantle to come from beneath North American continental lithosphere [see *Schellart et al.*, 2010 for further discussion of Farallon slab width in North America]. We propose that a similar increase in slab continuity may also have played a key role in the onset of root enhanced suction in South America, where the Farallon-Phoenix slab window was present beneath southern South America (Figure 3.5a) until ~53 Ma when the plates fused [*McCarron and Larter*, 1998].

We expect enhanced mantle wedge suction to be important for the northern half of South America, where the cratonic root has a larger and more continuous spatial extent and greater depth compared to the central and southern portions of the continent. The Eocene-Oligocene plate motion (Fig. 3.1 & 3.4) featured a northeast direction of subduction that placed the Central Andes between the Amazonian Craton and the down-going Nazca plate. At the end of the flat-slab period described in section 2.3.2, a major change in subduction obliquity occurred [*Somoza*, 1998]. Figure 3.1 and Figure 3.4f shows the plate configuration following the 25 Ma Nazca plate motion change. In the latter configuration, the Nazca plate was moving more directly toward the smaller and discontinuous Sao Francisco Craton, significantly different than the pre-25 Ma regime described above. As a result, suction in the mantle wedge would have been less intense, reducing lifting force and allowing steepening of the subduction angle.

### 3.2.2. Application to the Central Andes of South America

To model the dynamics of ~40 Ma and ~23 Ma subduction, we assume subducting slab and cratonic root geometries that allow estimation of the distance from

the mantle wedge tip to the craton at that time. A realistic model requires unbending of the Bolivian Orocline and restoring the western part of the Amazonian Craton root that probably was eroded during the course of slab-craton interaction. Figure 3.4 summarizes the information we use to construct the spatial scaling for our model.

We begin by restoring the subduction zone to the west (Figure 3.4a) so as to unrotate the post-45 Ma paleomagnetic rotations and shortening and straighten the subduction zone [Arriagada *et al.*, 2008; McQuarrie, 2002]. We do not account for subduction erosion of the forearc. To estimate the position of the mantle wedge tip, we use the location of 45 Ma and older volcanic arc rocks [Mamani *et al.*, 2010]. In Figure 3.4a, these rocks (blue) and the flat-slab region (yellow) of James and Sacks [1999] have been restored to their projected original locations according to the reconstruction of Arriagada *et al.* [2008]. Figure 3.4b shows the reconstruction for just after the 25-22 Ma plate motion change, where the mantle wedge tip is estimated by the position of 24-10 Ma arc rocks (orange, simplified from Mamani *et al.*, 2010).

To estimate the position of the craton edge, we start with the current-day craton edge, which we assume is represented by the western limit of >60 km elastic thickness [Pérez-Gussinyé *et al.*, 2008]. We expect that the modern craton does not represent the 45-40 Ma geometry, and assume that the base of the craton adjacent to the flat-slab was eroded during the ~10 m.y. of slab-craton interaction. The western portion of crustal Amazonian Craton lies in what was stable continent, so we assume the craton extended west to the margin of the crustally defined, exposed Proterozoic province [Figure 3.4, light grey, Fuck *et al.*, 2008; Bettencourt *et al.*, 2009]. For the ~40 Ma configuration, the distance between the mantle wedge tip and the craton edge is ~350 km (Figure 3.4a,

heavy black line). For the E-W oriented configuration, we choose the edge of the craton at ~25 Ma to match the elastic thickness curve (Figure 3.4b), resulting in a mantle wedge tip to craton edge distance of ~650 km.

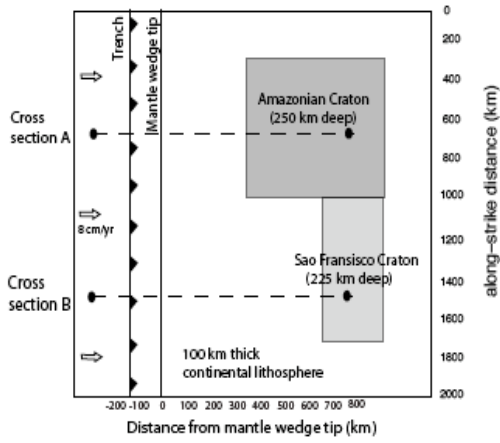
Following the modeling of *O'Driscoll et al.* [2009], we represent the Amazonian Craton (AC) and Sao Francisco Craton (SFC) to estimate slab-normal lifting force. The AC edge is positioned 350 km from the mantle wedge tip and has a maximum depth of 250 km (Figure 3.5a). The SFC is modeled as 650 km from mantle wedge tip and 225 km deep. Stress above the slab is resolved into a slab-normal component and integrated along the down dip length of the slab between 100 and 600 km depth. All other boundary conditions and material properties are identical to the reference models of *O'Driscoll et al.* [2009]. For reference, a continent without a lithosphere thicker than 100 km has an integrated slab-normal force of  $5.29 \times 10^{12}$  N/m, or 5.29 TN/m (Figure 3.5b).

Corresponding values for models in which the AC and SFC are included have maxima of 6.8 TN/m and 5.8 TN/m, respectively. Therefore, the additional suction due to the

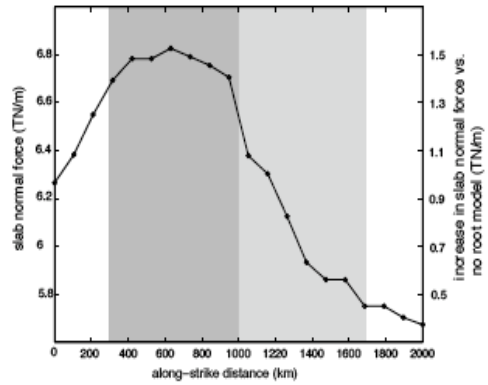
---

**Figure 3.5.** (next page) Finite element model representing South American cratonic configuration and comparison with our conceptual tectonic model. Model viscosity structure and boundary conditions provided in supplementary figure 1. (a) Map view of model configuration, note location of mantle wedge tip with respect to the AC and SFC. Location of cross sections shown in (c) and (d) given by dashed lines. (b) Integrated slab-normal stress between 100-600 km depth plotted versus along-strike distance. The dark grey and light grey represent the position of the AC and SFC, respectively. Absolute integrated force shown on left, the increase in suction compared to a reference rootless model shown on the right. (c) Cross section through modeled AC showing pressure field. Note the down-dip extent of the high-magnitude negative pressure. (d) Cross section through modeled SFC. (e-f) Illustrations of the context of modeling. Comparison of lithospheric configuration (e) pre-25 Ma Nazca obliquity change, where subduction beneath AC leads to strong enhanced suction above slab, indicated in yellow. (f) Post 25 Ma Nazca obliquity change, subduction was aligned with the distal SFC. The zone of enhanced mantle wedge suction was diminished. The change in plate motion is not modeled.

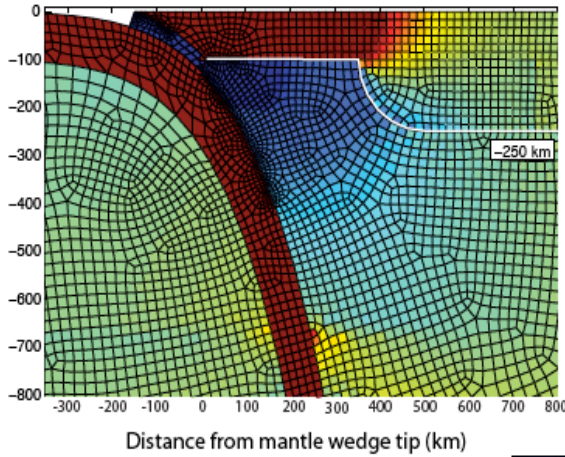
(a) 3D Model geometry



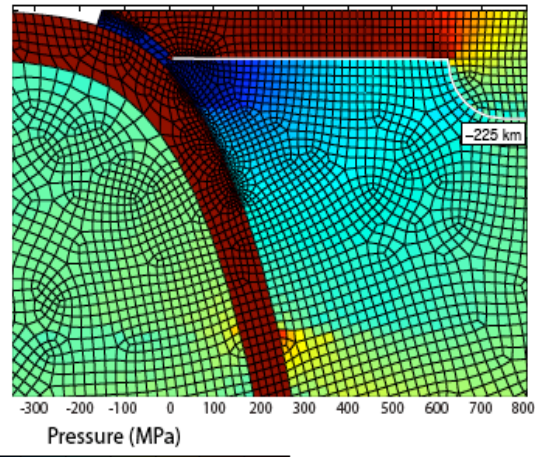
(b) Along-strike integrated slab normal force



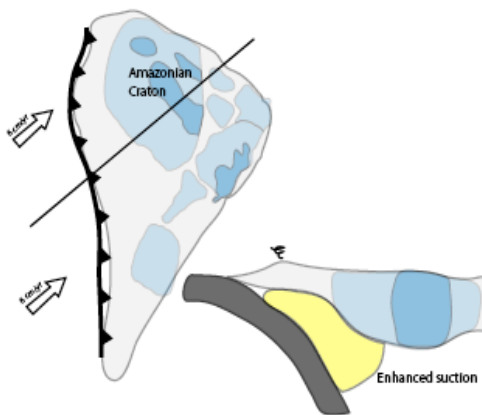
(c) Cross section A: Amazonian Craton



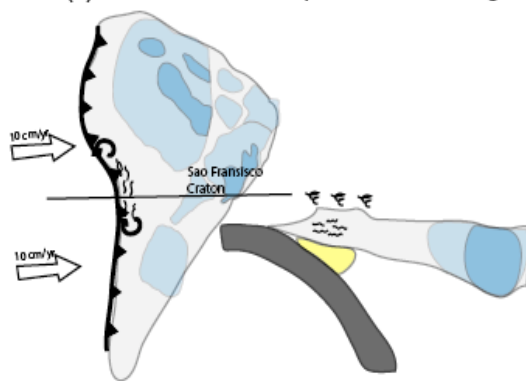
(d) Cross section B: Sao Francisco Craton



(e) 45 Ma, prior to flattening



(f) 24 Ma, after Nazca plate motion change



presence of the AC and SFC is calculated to be 1.51 TN/m and 0.51 TN/m, respectively. This modeling provides an estimate of the instantaneous forces acting on a subduction system, which is an underestimate, i.e., a lower bound: The root-enhanced suction will lift the slab by some amount, which in turn would cause an increase in suction and a progressive closure of the mantle wedge until a new equilibrium slab geometry is approached. Hence, the progressive closing of the mantle wedge and shallowing of the slab will serve to further enhance suction [e.g. *Stevenson and Turner, 1977; Tovish et al., 1978*].

### 3.3. Crustal buoyancy and oceanic plateau subduction

#### 3.3.1. Buoyant lithosphere subduction

Ocean plateau subduction has contributed to flat-slab formation and/or strong deformation of continental margins [*Gutscher et al., 2000*]. These plateaus are often formed at Large Igneous Provinces (LIP) that are constructed above increased mantle upwelling activity [*Richards et al., 1989*] or hot spot-spreading ridge interaction [e.g. *Ito et al., 1996*], and are characterized by thickened basaltic crust and depleted harzburgitic upper mantle. Some proposed examples include the ‘Lost Inca plateau’ subducted at the onset of the modern Peruvian flat-slab [*Gutscher et al., 1999*], the Yakutat terrane that currently subducts beneath the shallowly dipping and strongly shortening south Alaskan margin [*Christeson et al., 2010*], a subducted Shatsky Rise conjugate associated with the Laramide Orogeny [*Livacarrì et al., 1981; Saleeby, 2003; Liu et al., 2010*], and the Palau-Kyushu ridge that descends at the Nankai Trough, south Japan [*McGeary et al., 1985*].

The subduction of thick, buoyant oceanic lithosphere can aid in developing a shallow subduction angle [*van Hunen et al.*, 2002, 2004]. Anomalous buoyancy arises from the presence of metastable basalt is buoyant enough to reduced slab-pull force and allow mantle wedge suction to be more affective in establishing flatter slab geometry. However, plateau buoyancy alone does not cause slab flattening. *van Hunen et al.* [2004] conclude that either a high viscosity ( $>4 \times 10^{20}$  Pa-s) upper mantle (see also *Royden and Husson* [2006]) or strong overriding of continental lithosphere is required for oceanic plateau subduction to be successful in establishing a shallow angle slab. *Gerya et al.* [2009] show that for a slab to flatten due to positive buoyancy, the slab position must be near a threshold critical state owing to enhanced slab suction, overriding continental lithosphere, or other dynamic forces.

### 3.3.2. Manihiki plateau fragment subduction, Eocene Central Andes

Our plate motion reconstruction is consistent with the subduction of a Manihiki Plateau fragment (MPF) beneath the Central Andean margin around 40 Ma (Figure 3.6). Reconstruction of the MPF from just after its ~121 Ma creation at the PAC-FAR-PHX (PHP) triple junction [*Larson et al.*, 2002] to subduction beneath South America is provided using *Gplates* software [*Boyden et al.*, 2011]. The Manihiki Plateau, located below the SW Pacific Ocean, formed in association with extensive LIP growth in the Early Cretaceous, and is thought to be one of several large fragments that formed at the PFP ridge-ridge-ridge TJ [see Figure 3a in *Larson et al.*, 2002]. It has an estimated crustal thickness of 25 km [*Viso et al.*, 2005].

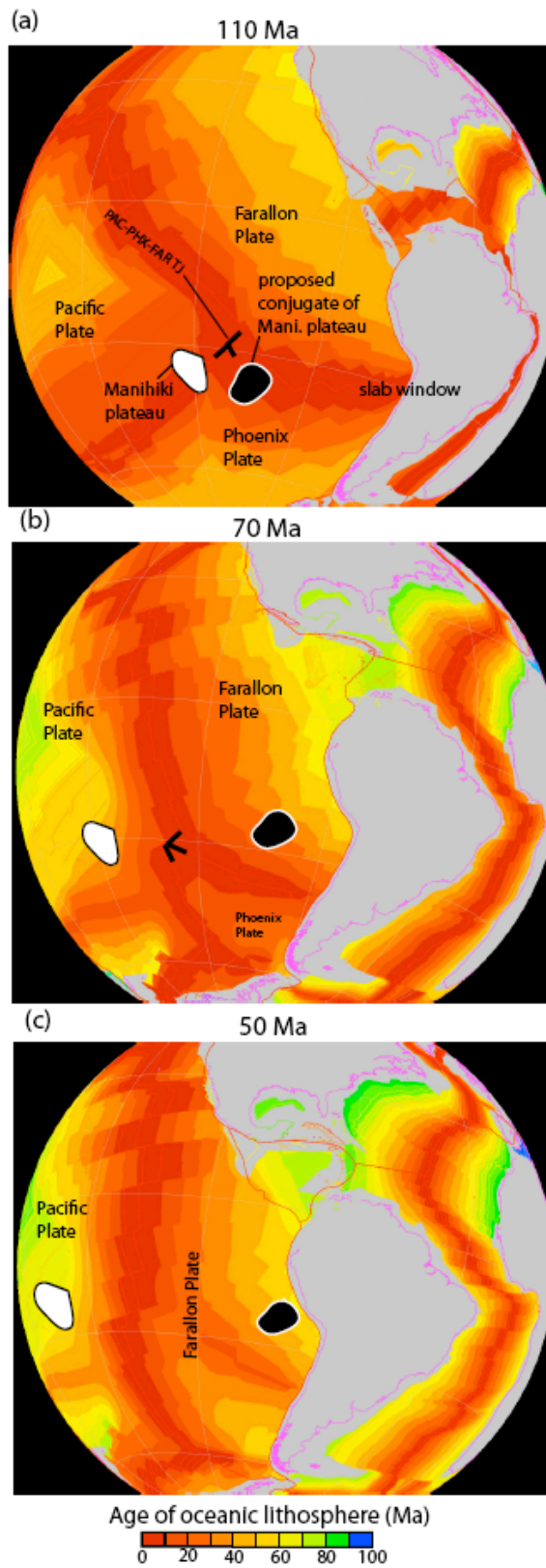
Collision of the MPF is best constrained in time and space by the locus of forearc block rotations and late Eocene flat-slab initiation. We infer that the onset of subduction of the MPF is indicated by intense shortening in Peru at ~45 Ma [*Benavides-Cáceras*, 1999] and Bolivia at ~40 Ma [*McQuarrie et al.*, 2005], and is consistent with pre-25 Ma formation of the Bolivian Orocline. Also, the period of decreased convergence rate noted by *Pardo-Casas and Molnar* [1987] is likely associated with subduction of buoyant oceanic lithosphere, a relationship consistent with the modeling of *Royden and Husson* [2009]. Reduction in dynamic support of the slab due to less vigorous corner-flow is a result of slowed convergence during plateau subduction [*Royden and Husson*, 2009; *Martinod et al.*, 2010]. *Martinod et al.* [2010] described the association between slowed convergence and the consumption of buoyant oceanic crust in South America, both for the modern flat-slab segments as well as the 37-25 Ma episode in the Central Andes.

### 3.3.3. Slab buoyancy estimate for the Manihiki Plateau

The plate reconstructions in Figure 3.6 show that ~50 m.y. old oceanic lithosphere created at the Phoenix-Farallon spreading center was subducting beneath Peru and

---

**Figure 3.6.** (next page) Reconstruction of the pathways of the Manihiki Plateau (white) and a conjugate fragment (black). (a) Cretaceous position of Pacific-Phoenix-Farallon triple junction and Manihiki plateau fragments ~10 m.y. after creation of the Manihiki LIP. A slab window beneath South America was present due to subduction of the Farallon-Phoenix spreading ridge. (b) Paleocene position of LIP fragments. The FAR-PHX spreading boundary was extinct, along with the corresponding slab window. (c) Eocene position of LIP fragments, the Manihiki conjugate is nearing interaction with Andean forearc.



Bolivia at 50-40 Ma (Fig. 3.5c). *Cloos* [1993] conclude that flat-slab formation is unlikely when the oceanic lithosphere >70 m.y. old subducts (~100 km thick lithosphere). Adding buoyancy to the slab, along with modulation of external stress, can establish a new equilibrium shape. To calculate a positive buoyancy force for the proposed subducted plateau in the late Eocene Central Andes, we use the 25 km crustal thickness for the Manihiki Plateau [*Viso et al.*, 2005]. Assuming a corresponding thickness of 65 km of a complementary harzburgite layer (following ratio of crust to harzburgite of *van Hunen et al.* [2004]), and densities of 2900 kg/m<sup>3</sup> (basalt), 3330 kg/m<sup>3</sup> (harzburgite), and 3400 kg/m<sup>3</sup> (peridotitic mantle), we estimate the positive buoyancy force of the 100 km thick slab with a buoyant plateau. For 100 km of subducted plateau (down dip length) we find a difference in density over 100 km thickness of 122 kg/m<sup>3</sup> and calculate ~1.22 TN/m of positive buoyancy. If we assume a more moderate crustal thickness of 15 km and 39 km harzburgite layer, the same calculation yields a density difference of 55 kg/m<sup>3</sup> and 0.55 TN/m of positive buoyancy. The 15 km thick plateau value we calculate is consistent with what *Gutscher et al.* [2000] calculated for the buoyancy of isostatically compensated columns of 50 m.y. old slabs with and without a buoyant plateau. Assuming compensation at 80 km depth in asthenosphere with a density of 3,230 kg/m<sup>3</sup>, they found a difference in buoyancy of 55 kg/m<sup>3</sup> for a plateau 2 km (a conservative representation of the Manihiki Plateau) above the 'normal' thickness oceanic lithosphere.

#### 3.4. Slab buoyancy vs. mantle wedge suction

The proposed late Eocene through late Oligocene flat-slab in the Central Andes occurred during a period without strong westward-directed continental overriding,

requiring an alternative mechanism for slab flattening. *van Hunen et al.* [2004] concludes that without continental overriding, only a combination of strong mantle suction and buoyant lithosphere subduction can lead to a flat subduction angle. This appears appropriate for the central Andes, where contributions of enhanced suction related to subduction beneath the cratonic structure of South America and positive buoyancy of a subducted oceanic plateau acted in concert. Plateau buoyancy has a local effect of slab lifting owing to the finite maximum along-strike width of plateau size with adjacent negatively buoyant slab. In comparison, cratonic continental lithosphere is as wide as 2000 km in Brazil, providing a slab lifting force along a much longer along-strike portion of the subducting slab. We examine the contributions to slab lifting in the local sense, finding that these two factors contribute about the same amount. However, considering the greater width of effective enhanced suction beneath a wide craton, we suggest that craton-slab interaction provides a dynamic stress configuration that can lead to slab flattening with added local perturbations such as buoyant lithosphere subduction.

We find the magnitude of added slab buoyancy to be of the same order of magnitude as the additional force due to slab suction induced by the nearby Amazonian Craton. Throughout the Mesozoic and Paleogene, subduction beneath the AC occurred without flat-slab formation, perhaps indicating that root-enhanced suction at minimum intensity, possibly due to along-strike flow coming from an adjacent slab window. We propose that with the arrival of the MPF, the combined forces of root-enhanced suction and plateau subduction were great enough to establish a new subduction geometry that included a flat-slab portion. As the subduction angle began to flatten, root-suction effects would have increased due to the approach of the slab to the root (Figure 3.5e). This is a

positive feedback mechanism that is expected to overcome the effect of decreasing convergence rate associated with the subduction of buoyant lithosphere [*Royden and Husson, 2006; Martinod et al., 2010*], which would otherwise diminish viscous flow in the mantle, and therefore diminish suction.

Further examination of the relative effects of enhanced mantle wedge suction and buoyant lithosphere subduction are warranted. *Manea et al. [2010]* investigated the time evolution of the subduction beneath central Chile by modeling the feedback between trench velocity and enhanced mantle wedge suction, finding that both great suction and a retreating trench are required for flat-slab development. We still do not fully understand the role of the subduction of positively buoyant, overthickened basaltic crust both in flattening in the uppermost mantle and in re-steepening the subduction angle upon conversion of basalt to eclogite. This crustal phase conversion may have played an important role in steepening the Central Andean slab, where the strong negative buoyancy of a thick eclogite layer may overwhelm the root suction force.

#### 4. COMPARISON BETWEEN THE SEVIER/LARAMIDE AND ANDEAN OROGENIES

The North American early Cenozoic Laramide Orogeny shares much in common with the tectonic activity that occurred along the Andean Cordillera [e.g. *Jordan and Allmendinger, 1986*], although there are important differences between these orogenies that may provide insight into the underlying processes. Both orogenies have been attributed to flat-slab subduction of ocean lithosphere beneath the continent, which shut

down arc magmatism and drove contemporaneous thrusting in the continental interior far from the subduction zone [e.g. *Jordan and Allmendinger, 1986; DeCelles, 2004*].

Three conditions are thought to be responsible for the occurrence and intensity of the Laramide: (1) acceleration of Farallon-North America convergence from 10 to 15 cm/yr during the 75-50 Ma interval [*Engebretson et al., 1985*], (2) the proximity of the large, thick Canadian Shield and the thick Proterozoic terrains accreted to its southern margin [*O'Driscoll et al., 2009*], and (3) relatively great slab buoyancy caused by plateau subduction and decreased lithosphere age. Laramide slab flattening and strongly contractional tectonism involved the end-on subduction of a large oceanic plateau (the conjugate of the Shatsky Rise, *Livacari et al., 1981, Liu et al., 2010; Saleeby, 2003*), which may have been larger than any of the plateaus and aseismic ridges involved with South American orogenesis.

The Laramide Orogeny was preceded by the 85 Ma and older Sevier Orogeny [e.g. *Taylor et al., 2000*], which affected the outboard margin of North America by developing a fold and thrust belt within thick Paleozoic sedimentary sequences. This orogeny produced a broad region of elevation gain [*Davis et al., 2009*] while arc magmatism remained active but migrated eastward [e.g., *DeCelles, 2004*]. The subsequent onset of the Laramide Orogeny is evidenced by the termination of magmatism and an eastward migration of thrusting into the continental interior, where crystalline basement was incorporated into the cores of the uplifts [e.g., *Livacari, 1991*]. This sequence of events occurred in a fairly continuous manner that can generally be described as a single orogenic event that grew in width, breadth and intensity over a ~50 m.y. duration.

Flat-slab subduction beneath South America was more irregular in its development and separate flattening events apparently involved only two of the three slab-flattening conditions that acted in concert during the Laramide. From the Miocene to present, slab flattening beneath central Chile is attributed to root-enhanced suction and rapid continental advance [*Manea et al.*, 2011], and beneath Peru it is attributed to subduction of buoyant oceanic lithosphere [*Gutscher et al.*, 1999] and continental advance. In contrast, the proposed Central Andes 37-25 Ma episode involved root suction and plateau subduction in the absence of rapidly advancing (overriding) continental plate. In the western U.S., the Laramide Orogeny was initiated by subduction of the Shatsky conjugate [*Livacarrì et al.*, 1981, *Liu et al.*, 2010; *Saleeby*, 2003], resulting in the strong deformation of a NE trending corridor from southern California through Wyoming. The progression of orogenic activity that occurred across this transect included strong erosion of the forearc (broken Salinian forearc, southern California), thin-skinned Sevier fold and thrust belt (Nevada and Utah) and Laramide affinity basement-cored uplifts (Utah, Colorado, and Wyoming) [*Saleeby*, 2003].

This suite of events in North America is similar to the transect across the Altiplano, including forearc deformation (Bolivian Orocline), fold and thrust belt development in thick Paleozoic sediments (Altiplano provinces; W. Cordillera, E. Cordilleran, InterAndean, SubAndean belts), and basement-cored uplifts (Sierra Pampeanas and Santa Barbara Range, Argentina). While the progression of events during the Andean Orogeny exhibited a similar outboard-to-inboard progression of deformation, these Andean provinces do not have the simple ‘corridor’ organization exhibited in the western U.S. *Capitanio et al.* [2011] attribute the inboard progression of deformation

focused across the Altiplano to dynamic effects excited by along-strike variations in plate strength as a function of the thickness of the continental lithosphere and age of the down-going oceanic lithosphere.

## 5. SOME REMARKS ON MODEL LIMITATIONS

Geodynamic modeling requires choosing specific sets of assumptions within which to derive results that may shed light on geological observations. Our models focus on how a subducting plate interacts with strong lithospheric roots adjacent to a continental margin, in particular, the forces resultant that may lead to flat-slab subduction. We also consider buoyancy effects due, e.g., to a subducted oceanic plateau. We rely on inferences from 3-D Cartesian mechanical models to help explain some of the spatial and temporal geologic relationships we highlight, particularly the history of flat-slab subduction, the magnitude and directions of relative plate motions, the history of crustal shortening, and the likely spatial distribution of deep continental roots. We have developed a model including inferred heterogeneity of the South American continental lithosphere thickness, and produce quantitative assessment of a tectonic contributor that can be inferred to play a role in Andean Orogeny evolution via the geologic record.

The dynamics of subduction is a complicated and many-faceted phenomenon. Given that all models of the subduction process are limited by simplifying assumptions and in terms of physical modeling capabilities, a degree of caution is warranted in interpreting these models. The models we have presented in this paper are by no means unique explanations for the set of tectonic observations we have summarized, and so are

perhaps best characterized as “quantitative plausibility arguments” deserving of more investigation.

As discussed in previous sections, other mechanisms have been proposed for flat slab subduction, and a number of important physical effects are absent in our 3-D Cartesian, instantaneous flow models: For example, two recent papers illustrate potentially important effects that we have not addressed, but which may affect Andean tectonics: subducted plate age [*Capitanio et al.*, 2011] and 3D sphericity effects [*Mahadevan et al.*, 2010] may influence both the subduction angle and trench morphology. However, we are not aware of any previous models that are able to explain the highly time-dependent and segmented nature of Cenozoic flat-slab subduction, as pointed out by *Capitanio et al.* [2011]. Furthermore, the sharp segmentation of flat-slab subduction, as well as its transient history beneath the Andes, suggests that the subducted Nazca/Farallon slab suffers highly-localized plastic failure, and hence is not likely a uniform or reliable transmitter of buckling stresses associated with the 3D spherical effects. Investigation of phenomena giving rise to this type of behavior is warranted in future geodynamic modeling.

## 6. CONCLUSIONS

The Central Andean flat-slab episode from 37-25 Ma marks a fundamental period of shortening that developed the Bolivian Orocline as well as crustal shortening that began construction of the early Altiplano. A strong correlation existed between the configuration of the South American lithosphere, the subduction obliquity and velocity, and the composition of the down-going oceanic lithosphere. We suggest that the

confluence of these dynamic effects induced sub-horizontal slab geometry in an absence of continental overriding. Furthermore, the orientation of subduction beneath the various portions of Precambrian shields appears to have both produced and ended flat subduction beneath the early Altiplano due to establishment and loss of enhanced mantle wedge suction, respectively. Higher resolution images of the lithospheric structure resulting from more complete seismic coverage of South America may allow a better understanding of the magnitude of the increase in mantle wedge suction.

We consider the multiple episodes of flattening that have occurred beneath both South and North America to be indicative of dynamic configurations favorable to flat-slab subduction that are related to slab-craton interaction. This may explain the observation that slab dips are on average shallower beneath continental than oceanic lithosphere [*Lallemand et al.*, 2005], with or without the influence of relatively buoyant subducted lithosphere.

Our tectonic model accounts for the pre-Miocene formation of the Arica Bend that is required by paleomagnetic rotation data [*Arriagada et al.*, 2008]. Further study of the 45-15 Ma period of rotation could much better constrain the timing of our proposed ocean plateau subduction. By placing the emphasis on this early phase of shortening in the central Andes, we are inherently supporting the model of protracted uplift history of the Altiplano [see *Barnes and Ehlers*, 2009, for discussion].

## CHAPTER IV

### TIME CORRECTIONS TO TELESEISMIC P DELAYS DERIVED FROM SKS

#### SPLITTING PARAMETERS

Reproduced with permission from Humphreys, E.; Schmandt, B.; *Geophysical Research Letters*, **2011**, 38, L19304. Copyright 2011, American Geophysical Union.

#### 1. INTRODUCTION

Although upper mantle anisotropy is common, as observed by its effects on surface waves and the splitting of S body waves, its effect on P-wave arrival times usually is ignored when tomographically inverting these times for structure [Sobolev *et al.*, 1999]. In well-studied areas such as the western U.S., observations on upper mantle anisotropy now are complete enough to allow for quantitative accounting of their effects on teleseismic P-wave arrival times. For this purpose, the most complete and useful data on upper mantle anisotropy are the split times and fast-axis orientations of SKS waves (e.g., Liu [2009], shown in Figure 4.1). Because SKS waves arrive with a steep inclination, the information they carry on anisotropy is limited to the elastic parameters that are sensitive to shear across a horizontal plane. Azimuthal anisotropy is thought to be the strongest part of upper mantle anisotropy in areas where horizontal flow is dominant [e.g., Vinnik *et al.*, 1989], and P waves will be delayed where this is the case. However, development of radial anisotropy near regions of vertical flow [Panning and Romanowicz, 2006] may cause a steeply inclined anisotropic fast axis, and then a strong P-wave advance and reduced SKS split times will result [Schulte-Pelkum and Blackman, 2003]. In transitional areas a fast-axis plunge can create complicated effects.

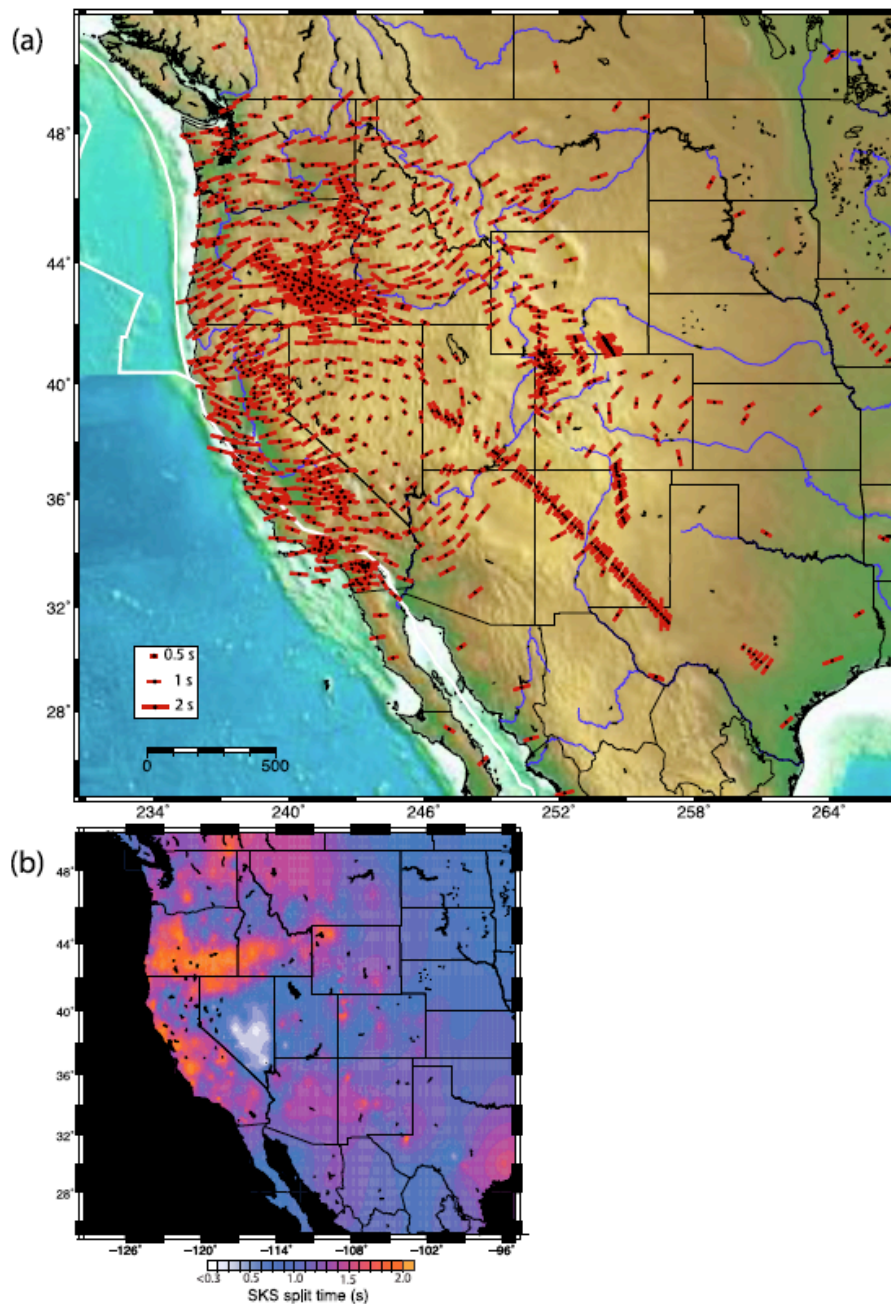


**Figure 4.1.** SKS field for the western U.S. Data compiled from *Liu* [2009], *Long et al.* [2009], *West et al.* [2009], *Eakin et al.* [2010], *Wang et al.* [2008], and *Satsukawa et al.* [2010]. (a) Station-averaged SKS split times (bar length, see key) and fast-axis orientations. (b) Interpolated SKS split-time magnitude, highlighting regions of strong splitting (e.g., High Lava Plains, southern Oregon) and minor splitting (central Great Basin, NV).

In this paper, we calculate a relation between SKS split time and the resulting P-wave travel-time correction assuming azimuthal anisotropy. We then use the splitting parameters derived from SKS arrivals recorded in the western U.S. to correct teleseismic P-wave arrival times for the effects of this anisotropy. The RMS of the travel-time corrections (0.16 s) is 37% of the data RMS, resulting in correction values large enough to change the form of tomographic inversions. Anisotropy not revealed by SKS splits is more difficult to resolve, but its effects on P delays may be even larger than those caused by azimuthal anisotropy.

## 2. TELESEISMIC P-WAVE CORRECTION TIMES BASED ON SKS SPLITTING PARAMETERS

Anisotropy of upper mantle peridotite has approximately hexagonal symmetry with a single fast axis. This characterization commonly is made because we typically cannot resolve any higher-order symmetry [Becker *et al.*, 2006], and the two slower axes tend to form a girdling pattern around the fast axis [Ismail and Mainprice, 1998] that has the effect of creating hexagonal symmetry. We follow Browaeys and Chevrot [2004] and decompose an olivine elastic tensor into an isotropic tensor plus a hexagonal perturbation tensor,

$$\mathbf{C}_{mn} = \begin{pmatrix} 195 & 67 & 67 & 0 & 0 & 0 \\ 67 & 195 & 67 & 0 & 0 & 0 \\ 67 & 67 & 195 & 0 & 0 & 0 \\ 0 & 0 & 0 & 64 & 0 & 0 \\ 0 & 0 & 0 & 0 & 64 & 0 \\ 0 & 0 & 0 & 0 & 0 & 64 \end{pmatrix} + \begin{pmatrix} -22 & 2 & -9 & 0 & 0 & 0 \\ 2 & -22 & 67 & 0 & 0 & 0 \\ -9 & 67 & 77 & 0 & 0 & 0 \\ 0 & 0 & 0 & -3 & 0 & 0 \\ 0 & 0 & 0 & 0 & -3 & 0 \\ 0 & 0 & 0 & 0 & 0 & -12 \end{pmatrix} . \quad (1)$$

We use the Voigt notation  $C_{mn} = c_{ijkl}$  where the subscripts on  $C$  represent elements of the elastic tensor  $c_{ijkl}$  following the convention for  $m$  and  $n$ : 1= $\Rightarrow$ 11, 2= $\Rightarrow$ 22, 3= $\Rightarrow$ 33, 4= $\Rightarrow$ 23 or 32, 5= $\Rightarrow$ 13 or 31, and 6= $\Rightarrow$ 12 or 21 (e.g.,  $C_{44} = c_{2323}$  and also  $c_{3232}$ ). The 3-axis is the fast axis. The effect of mixing olivine with orthopyroxene is well approximated simply by reducing the values in the hexagonal tensor [*Browaeys and Chevrot, 2004*]. The elastic constants in (1) are derived from lab experiments conducted at low pressure and temperature. A diminishing dominance of the hexagonal tensor over orthorhombic tensor occurs with depth, although, the hexagonal tensor of anisotropy remains stronger than the orthorhombic across the upper mantle [*Browaeys and Chevrot, 2004*]. All this is to say that our assumption of hexagonal symmetry captures the first-order effects of upper mantle anisotropy, and speaking practically, it is the best we can do in most situations.

To calculate travel time effects on teleseismic P arrivals, we further assume an upper mantle anisotropy with a horizontal fast axis (i.e., azimuthal anisotropy). The basis for this assumption is that with SKS observations we have insufficient information that can be used to recognize or constrain the angle of dip, and hence our assumption is the one of least bias. We discuss the implications of this assumption below.

With our representation of upper mantle anisotropy we now can calculate its effects on P-wave travel time. Compared to an isotropic mantle given by the isotropic elastic tensor in (1), a given teleseismic P-wave will be delayed by the presence of azimuthal anisotropy. Per unit distance, the P delay of a wave passing through anisotropic mantle, relative to that through an isotropic mantle, is  $(V_{\text{Panis}}^{-1} - V_{\text{Piso}}^{-1})$ . Similarly, the

SKS split time per unit distance is  $(V_{Sfast}^{-1} - V_{Sslow}^{-1})$  for the orthogonally polarized S waves. Thus the P-wave correction time  $t_P$  is related to split time  $\delta t_S$  by:

$$t_P = \delta t_S [(V_{Panis}^{-1} - V_{Piso}^{-1}) / (V_{Sfast}^{-1} - V_{Sslow}^{-1})]. \quad (2)$$

The ratio in brackets is independent of degree of anisotropy or material density, and only depends on the elasticity tensor and the propagation direction of the P and S waves with respect to this tensor (where, because anisotropy is weak, we assume that the difference group and phase wave velocities is negligible). Figure 4.2 shows values of this ratio as a function of ray inclination angle, for various back-azimuths with respect to the fast-axis azimuth. To determine this ratio, we calculate the split time (per unit distance) for SKS arrivals of  $10^\circ$  incidence angle, and average these split times over all back-azimuths. P-wave delays are then calculated for specified values of incidence angle and back-azimuth. In a location where a 1 second split time is observed, a vertically arriving P-wave would experience a 0.38 second delay under our assumptions (Figure 4.2).

### 3. WESTERN U.S. TELESEISMIC P-WAVE TRAVEL-TIME CORRECTIONS

To calculate P-wave travel-time corrections for the western U.S., we interpolate the SKS splitting parameters shown in Figure 4.1 onto a regular grid. Fast-axis azimuths are interpolated using the method of *Hansen and Mount* [1990]. Upper mantle anisotropy is represented by vertically projecting these results to depths of 100-300 km. Then a teleseismic ray set consisting of  $\sim 313,000$  rays [from *Schmandt and Humphreys, 2010a*] is traced through this structure and net P-wave travel-time correction is integrated using equation (2). These values are plotted as points in Figure 4.2 for incidence angles up to

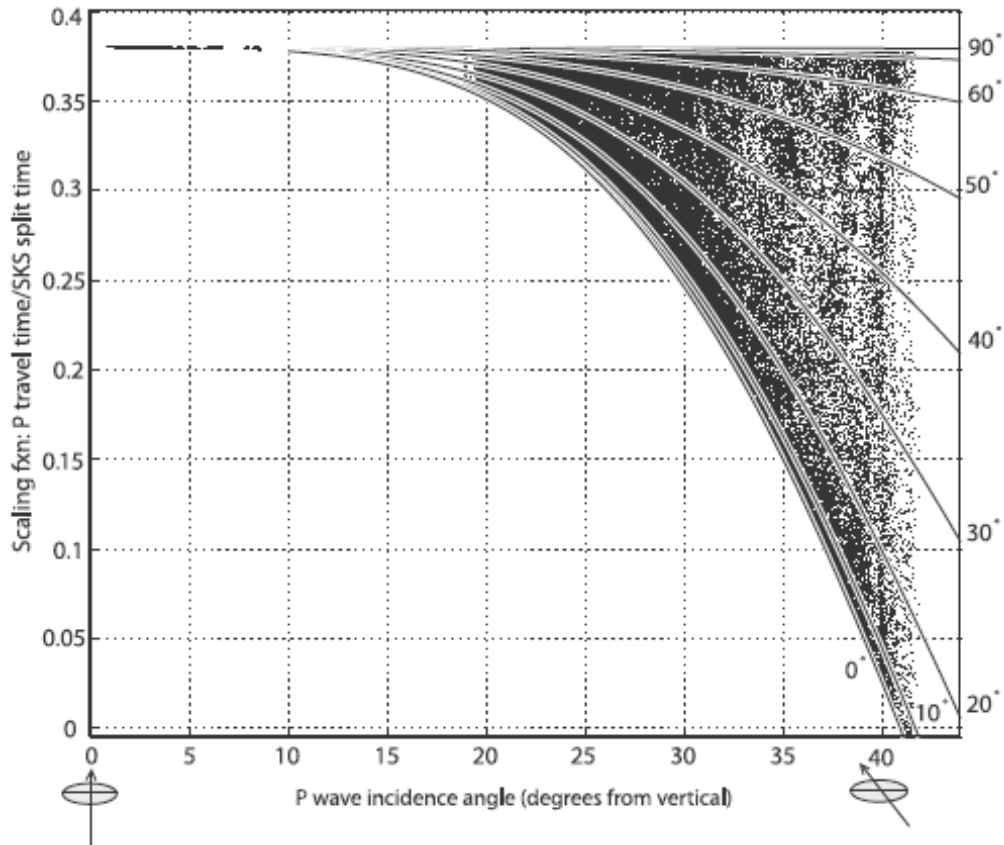


**Figure 4.2.** Ratio of P delay caused by azimuthal anisotropy to the SKS split time, as a function of P-wave incidence angle and back azimuth. Plotted curves represent the angular difference between ray back-azimuth and the SKS fast axis, ranging from  $90^\circ$  (ray is perpendicular to the fast axis) to  $0^\circ$  (ray in the vertical plane containing the fast axis, and approaches the fast axis with increasing incidence angle). Each dot represents one ray from our western U.S. ray set.

$\sim 43^\circ$ , and the demeaned results are shown as a map in Figure 4.3. The distribution of P-wave correction times is compared to the observed P-wave delays in the inset of Figure 4.3. The RMS of the correction times is 0.16 s, or 37% of the ray P-wave delay times. A correction of 0.3 s would alter the imaged P-wave velocity by  $\sim 1.2\%$  if the anisotropy were assumed to exist uniformly in a layer 200 km thick.

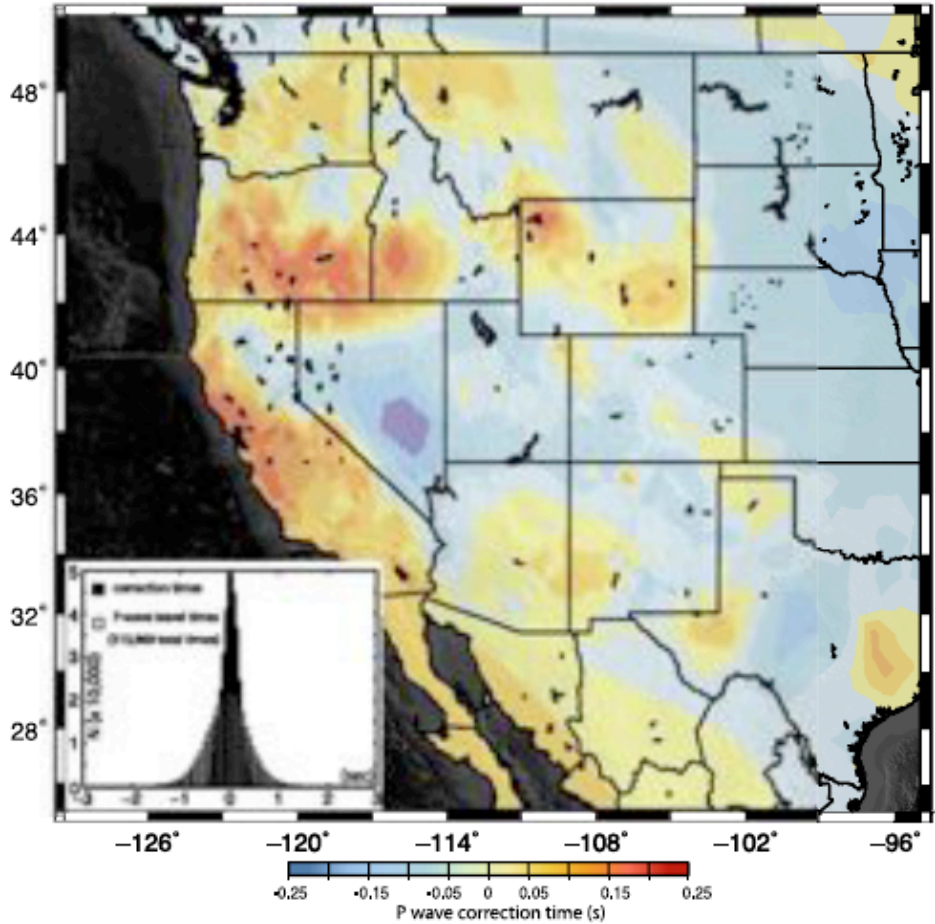


**Figure 4.3.** Interpolated map of P-wave arrival-time corrections estimated using the methods described in the text. A direct correlation between splitting magnitude and P-wave corrections is clear. (inset) Histograms of P-wave travel times (grey) and the corresponding estimated times (black) shown as dots in Figure 4.3. Data RMS is 0.437s, correction times RMS is 0.160s.

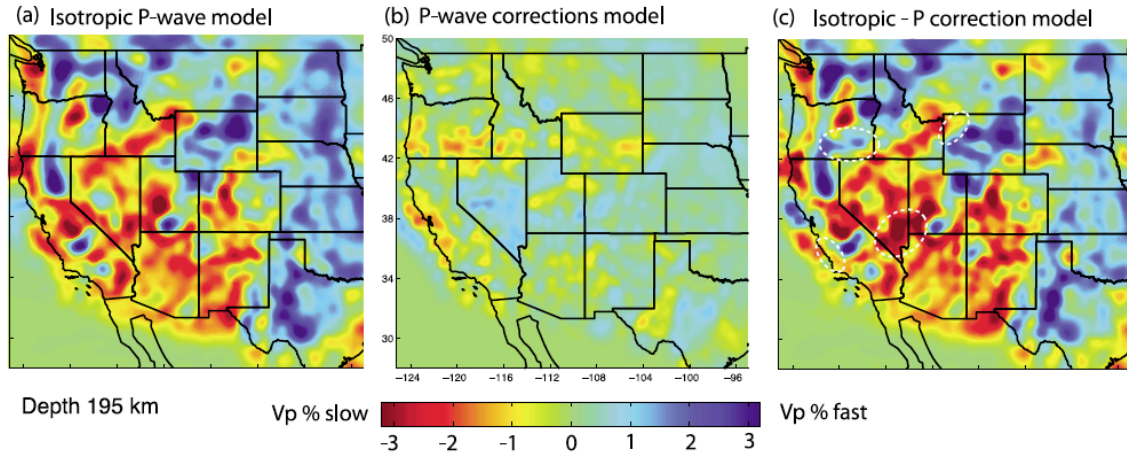
Figure 4.4a shows an isotropic P-wave inversion (i.e., ignoring anisotropy effects), following *Schmandt and Humphreys* [2010b]. Figure 4.4b is the result of inverting the SKS-based P-wave corrections, with strong damping at depths shallower than 90 km and deeper than 350 km. This damping effectively forces velocity structure to be created at lower lithosphere and asthenospheric depths. Figure 4c results from a subtraction of the model in Figure 4.4b from that of 4.4a. The dashed white ovals on

Figure 4.4c highlight some areas of significantly altered velocity, where the strong SKS splitting leads to faster velocities.

Figure 4.3 shows that SKS-based anisotropy delays define a prominent swath across the High Lava Plains of southern Oregon and the Snake River Plain of southern Idaho, where magmatism has been intense in the last 17 m.y. [*Christiansen and Yeats, 1992*]. Figure 4.4b shows that these corrections back-project constructively to depths of ~200 km. The Yellowstone area also shows SKS-based anisotropy delays, but these delays are imaged in the upper ~100 km indicating a more near-surface development of strong azimuthal anisotropy there. The other major area of correction delays is west-central California, and these delays also back-project constructively to ~200 km. This westernmost part of the NA plate is experiencing transform shear associated with the San Andreas Fault (SAF) system, and has recently experienced the withdrawal of the Juan de Fuca-Gorda slab [*Atwater, 1970*]. Beneath central Nevada, where splitting times are very small, are the most strongly negative P-wave corrections within the western U.S. These corrections back-project to ~200 km, suggesting little azimuthal anisotropy to these depths. This is an area where regional mantle downflow is expected owing to subduction and a hypothesized lithospheric instability [*Roth et al., 2008; West et al., 2009; Schmandt and Humphreys, 2010a*].

#### 4. DISCUSSION

We present a P-wave travel-time correction based on SKS split times under the assumption of azimuthal anisotropy, which is thought to dominate upper mantle anisotropy away from regions of downwelling such as subduction zones. In areas of large



**Figure 4.4.** Comparison of velocity models at 195 km depth. (a) Isotropic inversion of western U.S. P-wave travel-time data, including crustal corrections, following *Schmandt and Humphreys* [2010b]. (b) Inversion of only P-wave travel-time corrections shown in Figure 4.3. Inversion is damped to force structure between 90 and 350 km depths. (c) Difference between the isotropic model in (a) and the P delays inverted in (b). White ovals regions with the most obvious change in structure from (a).

split time observed over a range of back-azimuths, the fast axis of anisotropy is expected to be nearly horizontal, and the correction for P-wave delay probably is close to being correct. The back-azimuth dependence of this correction is then secondary to the magnitude in its effect on P-wave delay. However, when the fast axis has a moderate plunge, the effects on P-wave delays can be strongly back-azimuth dependent, and with moderate to vertical plunge the P-wave delays can be larger magnitude than those we calculate for azimuthal anisotropy [e.g., *Hartog and Schwarz, 2000; Schulte-Pelkum and Blackman, 2003*].

To illustrate the strong effect of a large fast-axis plunge angle, consider a subducted slab dipping at  $55^\circ$  similar to that of the imaged Gorda slab beneath northern California [*Schmandt and Humphreys, 2010b; Xue and Allen, 2010; Roth et al., 2008*]. Assuming the slab has an elastic tensor fast axis that plunges at the same angle, with an average anisotropy of 5%, we can estimate the P-wave delay with respect to isotropic

velocity. For waves arriving at  $\pm 25^\circ$  from vertical (typical teleseismic angle of incidence at 100 km depth) and in the plane normal to the strike of the slab, the delays caused by this anisotropy are -0.38 s (raypath subparallel to slab for  $\sim 300$  km) and 0.06 s (raypath  $\sim 120$  km across thickness of slab). Ignoring anisotropy would tend to make the slab too fast (to account for the rays that travel up the slab) and create zones paralleling the slab that are too slow (to account for the delayed arrivals that cross the anisotropic slab and account for the delays and to compensate for a slab that is too fast). This effect may be the source of a slab-parallel slow anomaly that lies beneath the entire along-strike length of the Juan de Fuca plate [Schmandt and Humphreys, 2010b; Xue and Allen, 2010; Roth et al., 2008].

With yet steeper plunge, SKS split times are small and P waves become strongly advanced. Eakin et al. [2010] discuss this correlation in the western U.S., which can be seen in Figure 4.4c. Thus, while split times will be small in areas where anisotropy is negligible (and P-wave correction times are close to zero), regions where small splits are common also could have vertical fast axes (and P-wave correction times should be maximal). In these cases, isotropic regions should have agreement between P and S models, whereas vertical anisotropy would create fast P-wave models compared to S-wave models. Also, nearly vertical anisotropy tends to align splitting orientation with the back-azimuth [Chevrot and van der Hilst, 2003]. This behavior is inconsistent with expectations of azimuthal anisotropy and can be mistaken for null results.

To illustrate this case we assume that the elastic tensor fast axis is vertical, such as may be expected above a detached and sinking piece of lithosphere. In this case the splitting of SKS would be small and a P wave would be advanced. Assuming a 5% fast

200 km of upper mantle, a P wave with an incidence angle of  $25^\circ$  would be advanced by  $\sim 0.3$  s compared to the isotropic case, whereas the corresponding direct S wave would be delayed by  $\sim 0.3$  s with respect to isotropic velocity. The result in a tomographic inversion would be a P-wave anomaly that is too fast and an S-wave anomaly that is too slow, and inconsistent estimates of SKS splitting with generally small split times. This is similar to what is imaged beneath northeast Oregon. There, a compact high-velocity structure is imaged at  $\sim 150$ - $300$  km depth that is thought to be a high-density, sinking body which is much stronger in the P-wave tomography than in the S-wave tomography [*Schmandt and Humphreys, 2010a*], and SKS arrivals are complex and the best-estimate split times are relatively small and fast axis azimuth is often ambiguous [*Long et al., 2009*].

## 5. CONCLUSION

We have estimated P-wave travel-time corrections based on SKS split times and applied these corrections to teleseismic P-waves recorded across the western U.S. Our considerations are limited to the effects of azimuthal anisotropy, which is thought to dominate upper mantle anisotropy away from regions of downwelling such as subduction zones. While only a part of the anisotropy effect, these correction times are significant.

Horizontal anisotropy inferred from SKS does not radically change western U.S. tomography, but the effect of the P-wave correction times is significant with respect to regional variations in upper mantle velocity. There are specific areas where these differences will influence the interpretations of mantle physical state and relation of mantle structure to surface activity (e.g., volcanism). Steeply plunging anisotropy is likely in regions of subduction [*Hartzog and Schwartz, 2000*], plumes [*Walker et al.,*

2005], and small-scale lithospheric downwellings [e.g. *Boyd et al.* 2004]. Hexagonal anisotropy predicts that such areas with plunging anisotropy could introduce more dramatic artifacts in isotropic travel-time tomography than those presented here.

## CHAPTER V

### CONCLUSIONS

I have examined the role of lithospheric heterogeneity within mountain belt evolution. The consideration of the variability of thickness and strength within all lithospheric plates is necessary to understand multi-scale processes in orogenesis, plate motion change, and to reconcile observations from the geologic record. The results from seismic imaging must also be viewed with careful consideration that the Earth is highly variable across many spatial scales.

Earth science is a relatively young science that underwent a major renewal with the development of the theory of plate tectonics in the 1960's and 1970's. The following few decades looked at validation of the theory. Great effort was taken to compile data and observations that were suitable for hypothesis testing. In the past few decades, increasing capacity for computer-based modeling simulations have began the process of significantly refining the plate tectonic theory. My work is one of many efforts consider the role of Earth's heterogeneous nature within the ongoing formulation of modern plate tectonic theory.

## REFERENCES CITED

### Chapter II

- Allmendinger, R.W., Jordan, T.E., Kay, S.M., Isacks, B.M., 1997, The evolution of the Altiplano-Puna Plateau of the central Andes, *Annual Review of Earth and Planetary Sciences*, 25, 139–174.
- Arcay, D., Lallemand, S., and Doin, M.-P., 2008, Back-arc strain in subduction zones: Statistical observations vs. numerical modeling, *Geochemistry, Geophysics Geosystems*, 9, Q05015, doi: 10/1029/2007GC001875.
- Billen, M., and Gurnis, M., 2001, A low viscosity wedge in subduction zones, *Earth and Planetary Science Letters*, 193, 227-236.
- Bird, P., 1988, Formation of the Rocky Mountains: A continuum computer model, *Science*, 239, 1501-1507.
- Bird, P., 1998, Testing hypotheses on plate-driving mechanisms with global lithosphere models including topography, thermal structure, and faults, *Journal of Geophysical Research*, 103, 10,115–10,129.
- Cadek, O., Fleitout, L., 2003, Effect of lateral viscosity variations in the top 300 km on the geoid and dynamic topography, *Geophysical Journal International*, 152, 566–580.
- Cande, S. C., Raymond, C. A., Stock, J. Haxby, W. F., 1995, Geophysics of the Pitman fracture zone and Pacific-Antarctic Plate motions during the Cenozoic, *Science*, 270, 947-953
- Engelbreton, D.C., Cox, A., Gordon, R.G., 1985, Relative motions between oceanic and continental plates in the Pacific basin, *GSA Special Paper* 206, 59p.
- English, J.M., Johnston, S.T., 2004, The Laramide Orogeny: What were the driving forces?, *International Geology Review*, 46, 833–838.
- Ferrari, L., 2006, Cenozoic evolution of the central part of the Mexican subduction zone from geologic and geophysical data in the eve of the result from the MASE experiment, *Eos Trans. AGU*, 87(52), Fall Meet. Suppl. Abstract T13F-01.
- Kim, Y., Greene, F., Espejo, L., Perez-Campos, X., Clayton, R., 2006, Receiver Function Analysis of the Middle American Subduction Zone in Central Mexico, *Eos Trans. AGU*, 87(52), Fall Meet. Suppl. Abstract T51B-0541.

- Grand, S.P., 1994, Mantle shear structure beneath the Americas and surrounding oceans, *Journal of Geophysical Research*, 99, 11,591–11,621.
- Gordon, R.G., and Jurdy, D.M., 1986, Cenozoic global plate motions, *Journal of Geophysical Research*, 91, 12,389–12,406.
- Gripp, A.E., Gordon, R.G., 2002, Young tracks of hotspots and current plate velocities, *Geophysical Journal International*, 150, 321–361.
- Gung, Y., Panning, M., Romanowicz, B., 2003, Global anisotropy and the thickness of continents, *Nature*, 422, doi:10.1038/nature01559
- Gutscher, M., Spakman, W., Bijwaard, H., Engdahl, E.R., 2000, Geodynamics of flat subduction; seismicity and tomographic constraints from the Andean margin, *Tectonics*, 19, 814–833
- Humphreys, E.D., Coblenz, D., 2007, North America dynamics and western U.S. tectonics, *Reviews of Geophysics*, 45, RG3001, doi:10.1029/2005RG000181
- Iaffaldano and Bunge, 2008, Strong plate coupling along the Nazca-South America convergent margin, *Geology*, 36, 443-446.
- Jarrard, R.D., 1986, Relations among subduction parameters, *Journal of Geophysical Research*, 24, 217–284.
- Kneller, E.A., and P.E. van Keken, 2008, The effects of three-dimensional slab geometry on deformation in the mantle wedge: implications for shear wave anisotropy, *Geochemistry, Geophysics, Geosystems*, 9, Q01003, doi:10.1029/2007GC001677, 2008.
- Lallemand, S., Heuret, A, Boutelier, D., 2005, On the relationships between slab dip, back-arc stress, upper plate absolute motion, and crustal nature in subduction zones, *Geochemistry Geophysics Geosystems*, 6, Q09006, doi:10.1029/2005GC000917.
- Lawver, L.A., R.D. Müller, 1994, Iceland hotspot track, *Geology*, 22, 311–314.
- Livaccari, R.F., Burke, K., Sengor, A.M.C., 1981, Was the Laramide orogeny related to subduction of an oceanic plateau?, *Nature*, 289, 276–278.
- Manea, V., and M. Gurnis, 2007. Subduction zone evolution and low viscosity wedges and channels, *Earth and Planetary Science Letters*, 264, 22-45.
- Manea, V., Manea, M., Kosoglodov, V., Sewell, G., 2006, Intraslab seismicity and thermal stress in the subducted Cocos plate beneath central Mexico, *Tectonophysics*, 420, 389-408.

- Müller, R.D., Sdrolias, M., Gaina, C. and Roest, W.R., 2008, Age, spreading rates and spreading asymmetry of the world's ocean crust, *Geochemistry, Geophysics, Geosystems*, 9, Q04006, doi:10.1029/2007GC001743.
- Pardo-Casas and Molnar, 1987, Relative motion of the Nazca (Farallon) and South American plates since Late Cretaceous time, *Tectonics*, 6, 233-248.
- Phipps-Morgan, J., Morgan, W.J., Zhang, Y.-S., Smith, W.H.F., 1995, Observational hints for a plume-fed sub-oceanic asthenosphere and its role in mantle convection, *Journal of Geophysical Research*, 100, 12753–12768, doi: 10.1029/95JB00041.
- Piomallo, C., Becker, T.W., Funiciello, F. Faccenna, C., 2006, Three-dimensional instantaneous mantle flow induced by subduction, *Geophysical Research Letters*, 33, L08304, doi:1029/2005GL025390.
- Ranalli, G., R. Pellegrini, S. D'Offizi, 2000, Time dependence of negative buoyancy and the subduction of continental lithosphere, *J. Geodynamics*, 30, 539-555.
- Ricard, Y., Doglioni, C., Sabadini, R., 1991. Differential rotation between lithosphere and mantle: a consequence of lateral mantle viscosity variations, *Journal of Geophysical Research*, 96, 8407–8415.
- Saleeby, J., 2003, Segmentation of the Laramide slab-evidence from the southern Sierra Nevada region, *Geological Society of America Bulletin*, 115, 655–668.
- Schellart, W.P., Freeman, Stegman, D.R., Moresi, L., May, D., 2006, Evolution and diversity of subduction zones controlled by slab width, *Nature*, 446, 308-311, doi:10.1038/nature05615.
- Silver, P.G., Russo, R.M., Lithgow-Bertelloni, C., 1998, Coupling of South American and African plate motion and plate deformation, *Science*, 279, 60–63.
- Sobolev, S.V., Babeyko, A.Y., 2003, What drives orogeny in the Andes?, *Geology*, 33, 617–620, doi:10.1130/G21557.1.
- Somoza, R., 1998, Updated Nazca (Farallon)-South America relative motions during the last 40 My: Implications for mountain building in the central Andean region, *Journal of South American Earth Science*, 11, 211–215.
- Stegman, D.R., Freeman, J., Schellart, W.P., Moresi, L., May, D., 2006, Influence of trench width on subduction hinge retreat rates in 3-D models of slab rollback, *Geochemistry Geophysics Geosystems*, 7, Q03012, doi:10.1029/2005GC001056.
- Stevenson, D.J., and Turner, J.S., 1977, Angle of subduction, *Nature*, v. 270, p. 334–336.

- Stock, J., Molnar, P., 1988, Uncertainties and implications of the late Cretaceous and Tertiary position of North America relative to the Farallon, Kula, and Pacific plates, *Tectonics*, 7, 1339–1384.
- Toomey, D.R., Wilcock, W.S.D., Conder, J.A., Forsyth, D.W., Blundy, J.D., Parmentier, E.M., Hammond, W.C., 2002, Asymmetric mantle dynamics in the MELT region of the East Pacific Rise, *Earth Planet. Sci. Lett.*, 200, 287–295.
- Tovish, A., Schubert, G., Luyendyk, B.P., 1978, Mantle flow pressure and the angle of subduction: Non-Newtonian corner flows, *Journal of Geophysical Research*, 83, 5892–5898.
- van Hunen, J., van den Berg, A.P., Vlaar, N.J., 2004, Various mechanisms to induce present-day shallow flat subduction and implications for the younger Earth: a numerical parameter study, *Physics of the Earth and Planetary Interiors*, 146, doi:10.1016/j.pepi.2003.07.027.
- Victor, P., Oncken, O., Glodny, J., 2004, Uplift of the western Altiplano plateau: Evidence from the Precordillera between 20° and 21°S (northern Chile), *Tectonics*, 23, TC4004, doi:10.1029/2003TC001519.
- Zhong, S., and Gurnis, M., 1995, Mantle convection with plates and mobile, faulted margins, *Science*, v. 276, p. 838-843, doi:10.1126/science.267.5199.838.

### Chapter III

- Arriagada, C., P. Roperch, C. Mpodozis, P. R. Cobbold (2008), Paleogene building of the Bolivian Orocline: Tectonic restoration of the central Andes in 2-D map view, *Tectonics*, 27, TC6014, doi:10.1029/2008TC002269
- Artemieva, I. M., W. D. Mooney (2001), Thermal thickness and evolution of Precambrian lithosphere: A global study, *J. of Geophys. Res.*, 106, 16,387-16,414
- Atherton, M. P. (1990), The Coastal batholith of Peru: The product of rapid recycling of “new” crust formed within rifted continental margin, *Geol. J.*, 25, 337-349
- Avila-Salinas, W. (1991), Petrologic and tectonic evolution of the Cenozoic volcanism in the Bolivian western Andes, *In: Harmon, R. S., C. W. Rapela (eds), Andean magmatism and its tectonic setting, Geological Society of America Special Paper 265, 279-290*
- Barazangi, M., B. L. Isacks (1976), Spatial distribution of earthquakes and subduction of the Nazca Plate beneath South America, *Geology*, 4, 686-692

- Barke, R., S. Lamb, C. MacNiocaill, (2007), Late Cenozoic bending of the Bolivian Andes: new paleomagnetic and kinematic constraints, *J. Geophys. Res.*, 112, doi:10.1029/2006JB004372
- Barnes, J. B., T. A. Ehlers, N. McQuarrie, P. B. O'Sullivan, S. Tawackoli (2008), Thermo-chronometer record of central Andean plateau growth, Bolivia (19.5°S), *Tectonics*, 27, TC3003, doi:10.1029/2007TC002174
- Benavides-Cáceres, V. (1999), Orogenic Evolution of the Peruvian Andes: The Andean Cycle, *In: Skinner, B., et al. (eds.) Geology and Mineral Deposits of Central Andes*, Society of Economic Geology, Special Publication, 7, 61-107
- Bettencourt, J. S., W. B. Leite Jr., A. S. Ruiz, R. Matos, B. L. Payolla, R. M. Tosdal (2010), The Rondonian-San Ignacio province in the SW Amazonian Craton: An overview, *J. S. Am. Sci.*, 29, 28-46, doi:10.1016/j.jsames.2009.08.006
- Bissig, T., T. D. Ullrich, R. M. Tosdal, R. Friedman, S. Ebert (2008), The time-space distribution of Eocene to Miocene magmatism in the central Peruvian polymetallic province and its metallogenetic implications, *J. of S. Am. Earth Sci.*, 26, 16-35, doi:10.1016/j.jsames.2008.03.004
- Boyden, J. A., R. D. Müller, M. Gurnis, T. H. Torsvik, J. A. Clark, M. Turner, G. Ivey-Law, R. J. Watson, J. S. Cannon (2011), Next-generation plate-tectonic reconstructions using Gplates, *Geoinformatics: Cyberinfrastructure for the Solid Earth Sciences*, G. R. Keller and C. Baru [eds], Cambridge University Press, *in press*
- Breitsprecher, K., D. J. Thorkelson, W. G. Groome, J. Dostal (2003), Geochemical confirmation of the Kula-Farallon slab window beneath the Pacific Northwest in the Eocene time, *Geology*, 31, 351-354, doi:10.1130/0091-7613(2003)031<0351:GCOTKF>2.0.CO;2
- Cahill, T., B. L. Isacks (1992), Seismicity and shape of the subducted Nazca plate, *J. Geophys. Res.*, 97, 17503-17529
- Capitanio, F. A., C. Faccenna, S. Zlotnik, D. R. Stegman (2011), Subduction dynamics and the origin of the Andean orogeny and the Bolivian orocline, *Nature*, 480, 83-86, doi:10.1038/nature10596
- Christeson, G. L., S. P. S. Gulick, H. J. A. van Avendonk, L. L. Worthington, R. S. Reece, T. L. Pavlis (2010), The Yakutat terrane: Dramatic change in crustal thickness across the Transition fault, Alaska, *Geology*, 38, 895-898, doi:10.1130/G31170.1

- Cloos, M. (1993), Lithospheric buoyancy and collisional orogenesis: Subduction of oceanic plateaus, continental margins, island arcs, spreading ridges, and seamounts, *Geol. Soc. Am. Bull.*, 105, 715-737
- Coney, P. J., C. A. Evenchick (1994), Consolidation of the American Cordilleras, *J. S. Am. Sci.*, 7, 241-262
- Davis, S. J., A. Mulch, A. R. Carroll, T. W. Horton, C. P. Chamberlain (2009), Paleogene landscape evolution of the central North American Cordillera: Developing topography and hydrology in the Laramide foreland, *Geol. Soc. Am. Bull.*, 121, 100-116, doi:10.1130/B26308.1
- DeCelles, P. G. (2004), Late Jurassic to Eocene evolution of the Cordilleran thrust belt and foreland basin system, western U.S.A., *Am. J. Sci.*, 304, 105-168
- Engebretson, D. C., A. Cox, R. G. Gordon (1985), Relative motions between oceanic and continental plates in the Pacific Basin, *Geol. Soc. Am. Spec. Pap.* 206
- English, J. M., S. T. Johnston (2004), The Laramide orogeny: What were the driving forces?, *Int. Geol. Rev.*, 46, 833-838, doi:10.2747/0020-6814.46.9.833
- Fuck, R. A., B. B. B. Neves, C. Schobbenhaus (2008), Rodinia descendants in South America, *Precam. Res.*, 160, 108-126, doi:10.1016/j.precamres.2007.04.018
- Gerya, T. V., D. Fossati, C. Cantieni, D. Seward, 2009, Dynamic effects of aseismic ridge subduction: numerical modeling, *European J. Min.*, 21, 649-661
- Gillis, R. J., B. K. Horton, M. Grove (2006), Thermo-chronology, geochronology, and upper crustal structure of the Cordillera Real: Implications for Cenozoic exhumation of the Central Andean Plateau, *Tectonics*, 25, Tc6007, doi:10.1029/2005TC001887
- Gurnis, M., M. Turner, S. Zahirovic, L. DiCaprio, S. Spasojevic, R. D. Müller, J. Boyden, M. Seton, V. C. Manea, D. J. Bower (2011), Plate tectonic reconstructions with continuously closing plates, *Computers & Geosciences*, doi:10.1016/j.cageo.2011.04.014
- Gotberg, N., N. McQuarrie, V. C. Caillaux (2010), Comparison of crustal thickening budget and shortening estimates in southern Peru (12-14°S): Implication for mass balance and rotations in the “Bolivian orocline,” *Geol. Soc. Am. Bull.*, 122, 727-742, doi:10.1130/B26477.1
- Gutscher, M. A., J. L. Olivet, R. M. Aslanian, J. P. Eissen (1999), The ‘lost Inca Plateau’: Cause of flat subduction beneath Peru?, *Earth Planet. Sci. Lett.*, 171, 335-341

- Gutscher, M. A., R. Maury, J. Eissen, E. Bourdon, 2000, Can slab melting be caused by flat subduction?, *Geology*, 28, 535-538
- Hammerschmidt, K., R. Döbel, H. Friedrichsen (1992), Implications of  $^{40}\text{Ar}/^{39}\text{Ar}$  data of Earlier Tertiary volcanic rocks from the north Chilean pre-Cordillera, *Tectonophysics*, 202, 55-81
- Haschke, M. R., E. Scheuber, A. Günther, K.-J. Reutter (2002), Evolutionary cycles during the Andean orogeny: repeated slab breakoff and flat subduction?, *Terra Nova*, 14, 49-55
- Heintz, M., E. Debayle, A. Vauchez (2005), Upper mantle structure of the South American continent and neighboring oceans from surface wave tomography, *Tectonophysics*, 406, 115-139, doi:10.1016/j.tecto.2005.05.006
- Hoke, L., D. Hilton, S. Lamb, K. Hammerschmidt, H. Friedrichson (1994),  $^3\text{He}$  evidence for a wide zone of active mantle melting beneath the Central Andes, *Earth Planet. Sci. Lett.*, 128, 341-355
- Horton, B. K., B. A. Hampton, G. L. Waanders (2001), Paleogene synorogenic sedimentation in the Altiplano Plateau and implications for initial mountain building in the Central Andes, *Geol. Soc. Am. Bull.*, 113, 1387-1400
- Isacks, B. (1988), Uplift of the Central Andean plateau and bending of the Bolivian orocline, *J. Geophys. Res.*, 93, 3211-3231
- Ito, G., J. Lin, C. W. Gable (1996), Dynamics of mantle flow and melting at a ridge-centered hotspot: Iceland and the Mid-Atlantic Ridge, *Earth and Plant. Sci. Lett.*, 144, 53-74, doi:10.1016/0012-821X(96)00151-3
- James, D. E., S. Sacks (1999), Cenozoic formation of the Central Andes: a geophysical perspective, *In: Skinner, B., et al. (eds.) Geology and Mineral Deposits of Central Andes*, Society of Economic Geology, Special Publication, 7, 1-25
- Jones, C. H., G. L. Farmer, B. Sageman, S. J. Zhong (2011), Hydrodynamic mechanism for the Laramide orogeny, *Geosphere*, 7, 183-201, 10.1130/GES00575.1
- Jordan, T. E., R. W. Allmendinger (1986), The Sierra Pampeanas of Argentina: A modern analogue of Rocky Mountain foreland deformation, *Am. J. of Sci.*, 286, 737-764
- Kay, S. M., J. M. Abbruzzi (1996), Magmatic evidence for Neogene lithospheric evolution of the central Andean "flat-slab" between 30°S and 32°S, *Tectonophysics*, 259, 15-28

- Kay, S. M., V. MaksaeV, R. Moscoso, C. Mpodozis, C. Nasi (1987), Probing the evolving Andean lithosphere: Mid-late Tertiary magmatism in Chile (29°-30°30'S) over the modern zone of subhorizontal subduction, *J. Geophys. Res.*, 92, 6173-6189
- Kay, S. M., C. Mpodozis, B. Coira (1999) Neogene magmatism, tectonism, and mineral deposits of the Central Andes (22°S to 33°S), *In: Skinner, B., et al. (eds.) Geology and Mineral Deposits of Central Andes*, Society of Economic Geology, Special Publication, 7, 27-59
- Lallemand, S., A. Heuret, D. Boutelier (2005), On the relationships between slab dip, back-arc stress, upper plate absolute motion, and crustal nature in subduction zones, *Geochem. Geophys. Geosystems*, 6, 9, doi:10.1029/2005GC000917
- Lahsen, A. (1982), Upper Cenozoic volcanism and tectonism in the Andes of northern Chile, *Earth Sci. Rev.*, 18, 285-302
- Lamb, S., L. Hoke (1997), Origin of the high plateau in the Central Andes, Bolivia, South America, *Tectonics*, 16, 623-649
- Larson, R. L., R. A. Pockalny, R. F. Viso, E. Erba, L. J. Abrams, B. P. Luyendyk, J. M. Stock, R. W. Clayton (2002), Mid-Cretaceous tectonic evolution of the Tongareva triple junction in the southwestern Pacific Basin, *Geology*, 30, 67-70
- Liu, L., M. Gurnis, M. Seton, J. Saleeby, R. D. Müller (2010), The role of oceanic plateau subduction in the Laramide orogeny, *Nature Geoscience*, 3, 353-357, doi:10.1038/NGEO829
- Livacarrì, R. F., K. Burke, A.M.C. Sengor (1981), Was the Laramide Orogeny related to subduction of an oceanic plateau?, *Nature*, 289, 276-278, doi:10.1038/289276a0
- Livacarrì, R. F. (1991), Role of crustal thickening and extensional collapse in the tectonic evolution of the Sevier-Laramide orogeny, western United States, *Geology*, 19, 1104-1107, doi:10.1130/0091-7613(1991)019<1104:ROCTAE>2.3.CO;2
- Mahadevan, L., R. Bendick, H. Liang (2010), Why subduction zones are curved, *Tectonics*, 29, TC6002, doi:10.1029/2010TC002720
- Manea, V. C., M. Pérez-Gussinyé, M. Manea (2011), Chilean flat-slab subduction controlled by overriding plate thickness and trench rollback, *Geology*, 40, 35-38, doi:10.1130/G32543.1
- Mamani, M., G. Wörner, T. Sempere (2010), Geochemical variations in igneous rocks of the Central Andean orocline (13°S to 18°S): Tracing crustal thickening and magma generation through time and space, *Geol. Soc. Am. Bull.*, 122, 162-182, doi:10.1130/B26538.1

- Martinod, J., L. Husson, P. Roperch, B. Guillaume, N. Espurt (2010), Horizontal subduction zones, convergence velocity and the building of the Andes, *Earth Planet. Sci. Lett.*, 299, 299-309, doi:10.1016/j.epsl.2010.09.010
- McCarron, J. J., R. D. Larter (1998), Late Cretaceous to early Tertiary subduction history of the Antarctic Peninsula, *J. Geol. Soc. London*, 155, 255-268, doi:10.1144/gsjgs.155.2.025
- McGeary, S., A. Nur, Z. Ben-Avraham (1985), Spatial gaps in arc volcanism: the effect of collision or subduction of oceanic plateaus, *Tectonophysics*, 119, 195–221
- McQuarrie, N. (2002), Initial plate geometry, shortening variations, and evolution of the Bolivian orocline, *Geology*, 30, 867-870
- McQuarrie, N., J. M. Stock, C. Verdel, B. P. Wernicke, (2003), Cenozoic evolution of Neotethys and implications for the causes of plate motions, *Geophys. Res. Lett.*, 30, doi:10.1029/2003GL017992
- McQuarrie, N., B. K. Horton, G. Zandt, S. Beck, P. G. DeCelles (2005), Lithospheric evolution of the Andean fold-thrust belt, Bolivia, and the origin of the central Andean plateau, *Tectonophysics*, 399, 15-37, doi: 10.1016/j.tecto.2004.12.013
- McQuarrie, N., J. B. Barnes, T. A. Ehlers (2008), Geometric, kinematic, and erosional history of the central Andean Plateau, Bolivia (15-17°S), *Tectonics*, 27, TC3007, doi:10.1029/2006TC002054
- O'Connor, J. M., R. A. Duncan (1990), Evolution of the Walvis Ridge-Rio Grande Rise hot spot system: Implications for African and South American plate motions over plumes, *J. Geophys. Res.*, 95, 17475-17502
- O'Driscoll, L. J., E. D. Humphreys, F. Saucier (2009), Subduction adjacent to deep continental roots: Enhanced negative pressure in the mantle wedge, mountain building and continental motion, *Earth Planet. Sci. Lett.*, 280, 61-70, doi:10.1016/j.epsl.2009.01.020
- Oncken, O., D. Hindle, J. Kley, K. Elger, P. Victor, K. Schemmann (2006), Deformation of the central Andean upper plate system — facts, fiction, and constraints for plateau models, *In: Oncken, O., et al. (Eds.), The Andes: Active Subduction Orogeny*. Springer- Verlag, Berlin, 3–27.
- Pardo-Casas, F., P. Molnar (1987), Relative motion of the Nazca (Farallon) and South American plates since Late Cretaceous time, *Tectonics*, 6, 233-248
- Pérez-Gussinyé, M., A. R. Lowry, J. Phipps Morgan, A. Tassara (2008), Effective elastic thickness variations along the Andean margin and their relationship to subduction geometry, *Geochem. Geophys. Geosys.*, 9, Q02003, doi:10.1029/2007GC001786



- Schellart, W. P., D. R. Stegman, R. J. Farrington, J. Freeman, L. Moresi (2010), Cenozoic tectonics of western North America controlled by evolving width of Farallon slab, *Science*, 329
- Schobbenhaus, C., J. H. Goncalves, J. O. S. Santos, M. B. Abram, R. Leão Neto, G. M. M. Matos, R. M. Vidotti, M. A. B. Ramos, J. D. A. Jesus (2004), *Geological Map of Brazil*, 46 map sheets at 1:1,000,000 scale, Geographic Information System – GIS, Geologic Survey of Brazil-CPRM, Brasilia, 41 CD-ROM
- Sempere, T., R. F. Bulter, D. R. Richards, L. G. Marshall, W. Sharp, C. C. Swisher (1997), Stratigraphy and chronology of late Cretaceous-early Paleogene strata in Bolivia and northern Argentina, *Geol. Soc. Am. Bull.*, 109, 709-727
- Silver, P. G., R. M. Russo, C. Lithgow-Bertelloni (1998), Coupling of South American and African Plate Motion and Plate Deformation, *Science*, 279, 60-63
- Sobolev, S. V., A. Y. Babeyko (2005), What drives orogeny in the Andes?, *Geology*, 33, 617-620, doi:10.1130/G21557.1
- Somoza, R. (1998), Updated Nazca (Farallon)-South America relative motions during the last 40 My: implications for mountain building in the central Andean region, *J. S. Am. Sci.*, 11, 211-215
- Stevenson, D. J., S. J. Turner (1977), Angle of subduction, *Nature*, 270, 334-336
- Taylor, W. J., J. M. Bartley, M. W. Martin, J. W. Geissman (2000), Relations between hinterland and foreland shortening: Sevier orogeny, central North American Cordillera, *Tectonics*, 19, 1124-1143
- Tebbens, S., S. Cande (1997), Southeast Pacific tectonic evolution from Early Oligocene to present, *J. Geophys. Res.*, 102, 12061-12059
- Tovish, A., G. Schubert, B. P. Luyendyk (1978), Mantle flow pressure and the angle of subduction: non-Newtonian corner flows, *J. Geophys. Res.*, 83, 5892-5898
- van Hunen, J., A. P. van den Berg, N. J. Vlaar (2002), On the role of subducting oceanic plateaus in the development of shallow flat subduction, *Tectonophysics*, 352, 317-333
- van Hunen, J., A. P. van den Berg, N. J. Vlaar (2004) Various mechanisms to induce present-day shallow flat subduction and implications for the younger Earth: a numerical parameter study, *Phys. Earth Planet. Interiors*, 146, 179-194, doi:10.1016/j.pepi.2003.07.027
- Vlarr, N. J. (1983), Thermal anomalies and magmatism due to lithospheric doubling and shifting, *Earth Planet. Sci. Lett.*, 65, 322-330

Viso, R. F., R. L. Larson, R. A. Pockalny (2005), Tectonic evolution of the Pacific-Phoenix-Farallon triple junction in the South Pacific Ocean, *Earth Planet. Sci. Lett.*, 233, 179-194

#### **Chapter IV**

Atwater, T. (1970), Implications of plate tectonics for the Cenozoic tectonic evolution of western North America, *Bull. Geol. Soc. Amer.*, 81, 3513-3536

Becker, T. W., S. Chevrot, V. Schulte-Pelkum, D. K., Blackman (2006), Statistical properties of seismic anisotropy predicted by upper mantle geodynamic models, *J. Geophys. Res.*, 111, B08309, doi:10.1029/2005JB004095

Boyd, O. S. C. H. Jones, A. F. Sheehan (2004), Foundering lithosphere imaged beneath the southern Sierra Nevada, California, USA, *Science*, 305, 660-662

Browaeys, J. T., S. Chevrot (2004), Decomposition of the elastic tensor and geophysical applications, *Geophys. J. Int.*, 159, 667-678, doi:10.1111/j.1364-246X.2004.02415.x

Chevrot, S., R. D. van der Hilst (2003), On the effects of a dipping axis of symmetry on shear wave splitting measurements in a transversely isotropic medium, *Geophys. J. Int.*, 152, 497-505

Christiansen, R. L., and Yeats, R. L. (1992), Post-Laramide geology of the U.S. Cordillerian region, in Burchfiel, B. C., Lipman, P. W., and Zoback, M. L., eds., *The Cordillerian Orogen: Conterminous U.S.: Boulder, CO, Geological Society of America, Geology of North America: v. G-3, p. 261-406.*

Eakin, C. M., M. Obreski, R. M. Allen, D. C. Boyarko, M. R. Brudzinski, R. Porritt (2010), Seismic anisotropy beneath Cascadia and the Mendocino triple junction: Interaction of the subducting slab with mantle flow, *Earth and Planetary Science Letters*, 297, 627-632, doi:10.1016/j.epsl.2010.07.015

Hansen, K. M., and V. S. Mount (1990), Smoothing and extrapolation of crustal stress orientation measurements, *J. Geophys. Res.*, 95, 1155-1165

Harzog, R., S. Y. Schwartz (2000), Subduction-induced strain in the upper mantle east of the Mendocino Triple Junction, California, *J. Geophys. Res.*, 105, 7909-7930

Ismail, W. B., D. Mainprice (1998), An olivine fabric database: an overview of upper mantle fabrics and seismic anisotropy, *Tectonophys.*, 296, 145-157

- Liu, K. H., (2009), NA-SWS-1.1: A uniform database of teleseismic shear wave splitting measurements for North America, *Geochem. Geophys. Geosys.*, 10, Q05011, doi:10.1029/2009GC002440
- Long, M. D., H. Gao, A. Klaus, L. S. Wagner, M. J. Fouch, D. E. James, E. Humphreys (2009), Shear wave splitting and the pattern of mantle flow beneath eastern Oregon, *Earth and Planetary Science Letters*, 288, 359-369, doi:10.1016/j.epsl.2009.09.039
- Panning, M. B. Romanowicz (2006), A three-dimensional radially anisotropic model of shear velocity in the whole mantle, *Geophys. J. Int.*, 167, 361-379, doi:10.1111/j.1365-246X.2006.03100.x
- Roth, J. B., M. J. Fouch, D. E. James, R. W. Carlson (2008), Three-dimensional seismic velocity structure of the northwestern United States, *Geophys. Res. Lett.*, 7, 417-420
- Satsukawa, T. K. Michibayashi, U. Raye, E. Y. Anthony, J. Pulliam, R. Stern (2010), Uppermost mantle anisotropy beneath the southern Laurentian margin: Evidence from Knippa peridotite xenoliths, Texas, *Geophys. Res. Lett.*, 37, L20312, doi:10.1029/2010GL044538
- Schmandt, B., E. Humphreys (2010a), Complex subduction and small-scale convection revealed by body-wave tomography of the western United States upper mantle, *Earth and Planetary Science Letters*, 297, 435-445, doi:10.1016/j.epsl.2010.06.047
- Schmandt, B., E. Humphreys, (2010b), Seismic heterogeneity and small-scale convection in the southern California upper mantle, *Geochem. Geophys. Geosys.*, 11, Q05004, doi:10.1029/2010GC003042
- Schulte-Pelkum, V., D. K. Blackman (2003), A synthesis of seismic P and S anisotropy, *Geophys. J. Int.*, 154, 166-178
- Sobolev, S. V., A. Grésillaud, M. Cara (1999), How robust is isotropic delay time tomography for anisotropic mantle?, *Geophys. Res. Lett.*, 26, 509-512
- Vinnik, L. P., V. Farra, and B. Romanowicz (1989), Azimuthal anisotropy in the Earth from observations of SKS at Geoscope and NARS broadband stations, *Bull. Seismol. Soc. Am.*, 79, 1542-1558
- Wang, X., J. F. Ni, R. Aster, E. Sandvol, D. Wilson, C. Sine, S. P. Grand, W. S. Baldrige (2008), Shear-wave splitting and mantle flow beneath the Colorado Plateau and its boundary with the Great Basin, *Bulletin of the Seismological Society of America*, 98(5), 2526-2532, doi:10.1785/0120080107
- Walker, K. T., G. H. R. Bokelmann, S. L. Klemperer, G. Bock (2005), Shear-wave splitting around the Eifel hotspot: evidence for a mantle upwelling, *Geophys. J. Int.*, 163, 962-980

West, J. D., M. J. Fouch, J. B. Roth, L. T. Elkins-Tanton (2009), Vertical mantle flow associated with a lithospheric drip beneath the Great Basin, *Nature Geoscience*, 2, 439-444, doi:10.1038/NGEO526

Xue, M. and R. M. Allen (2010), Mantle structure beneath the Western US and its implications for convection processes, *J. Geophys. Res.*, 115, B07303, doi:10.1029/2008JB006079.